Western Area, Pb element is concentrated in the acidic volcanic (Ivv and Ivt) in the Western Area and intrusive rocks, and Zn element is concentrated more than average value in the formations of IIap and Iiat in the Eastern Area and in the formation of Ic, Ivt, Ivv and Ips in the Western Area.

(4) Variation of Geochemical Values and Geologic Structure

The variation of geochemical values of rock samples as well as gossan samples along 6 sampling lines are sown in the Fig. I-25. The location of the sampling lines are shown in the Fig. I-21 and Fig. I-22.

In the sampling line of the Imarine area (1), the variation of metal contents controlled by rock formation is small and the sample around fault in the center of the line shown high values of Zn and Ag. In the Amzourh area (2), near the both ends of the sampling line, Cu, Pb, and Zn show high values which seems to be affected by fault fractures.

In the Oukhribane-Akhlij area (3), at the southwestern end of the survey line, high values of Cu, Pb and Ag are found in the formation IIaa. It is inferred to be influenced by the mineralization because average metal contents of the formation IIaa is not high usually.

In the Frizem Area (4, 5, 6), gossan samples show high metal contents affected by the mineralization of the eastern dissemination ore and the western vein-shaped ore.

3-4 Interpretation

According to the concentration degree of metal elements in each formation, Cu and Zn are concentrated in the tuffaceos green rock (IIat) in the Oukhribane Block. This fact suggests that the tuffaceous green rock is equivalent to the mineralized horizon of stockwork ore developed

at the lower part of the massive ore at the Hajar ore deposit.

Pb and Zn are concentrated in the acidic volcanic rocks in the Frizem Area. It suggests that the rocks have some intimate relation with the Pb-Zn mineralization in this area.

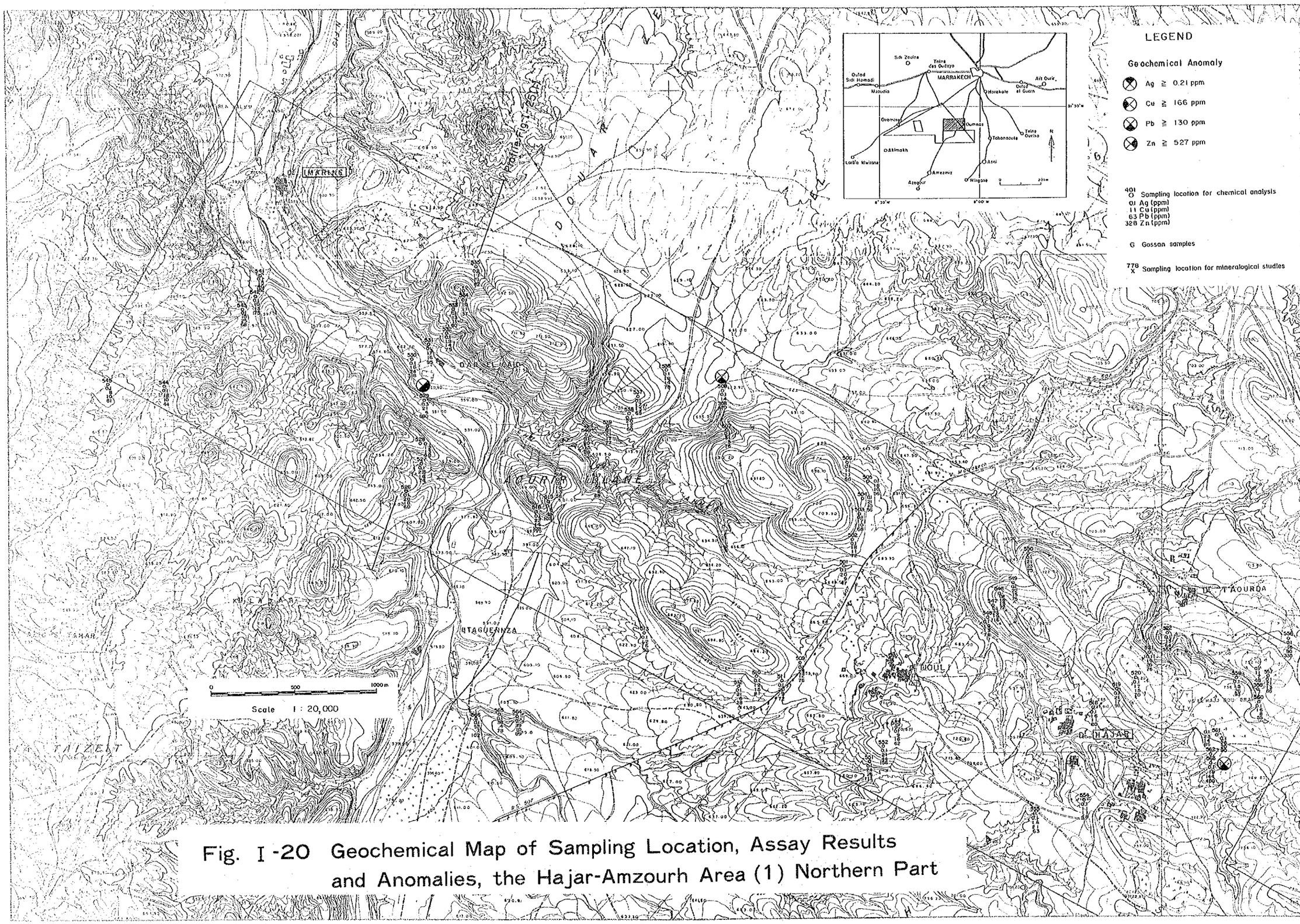
LEGEND
Geochemical Anomaly
Ag ≧ 0.21 ppm
Cu ≧ 166 ppm
Pb ≧ 130 ppm
Zn ≧ 527 ppm
401 O Sampling location for chemical analysis
01 Ag (ppm)
11 Cu (ppm)
63 Pb (ppm)
328 Zn (ppm)
G Gossan samples
778 X Sampling location for mineralogical studies
MARRAKECH
Sidi Zouine
Tnine des Oudaya
Oulad Sidi Hamadi
Mzoudia
Harakate
Ait Ourir
Ouled al Guzzn
Guemassa
Oumnas
Tahanaoute
Tnine Ourika
Oukimakh
Larba Nkirzna
Asni
Arrezmz
Azegour
Wirgane
8°30'W
8°00'W
31°30'N
0 20km
N
Scale 1 : 20,000
0 500 1000m
Fig. I-20 Geochemical Map of Sampling Location, Assay Results and Anomalies, the Hajar-Amzourh Area (1) Northern Part

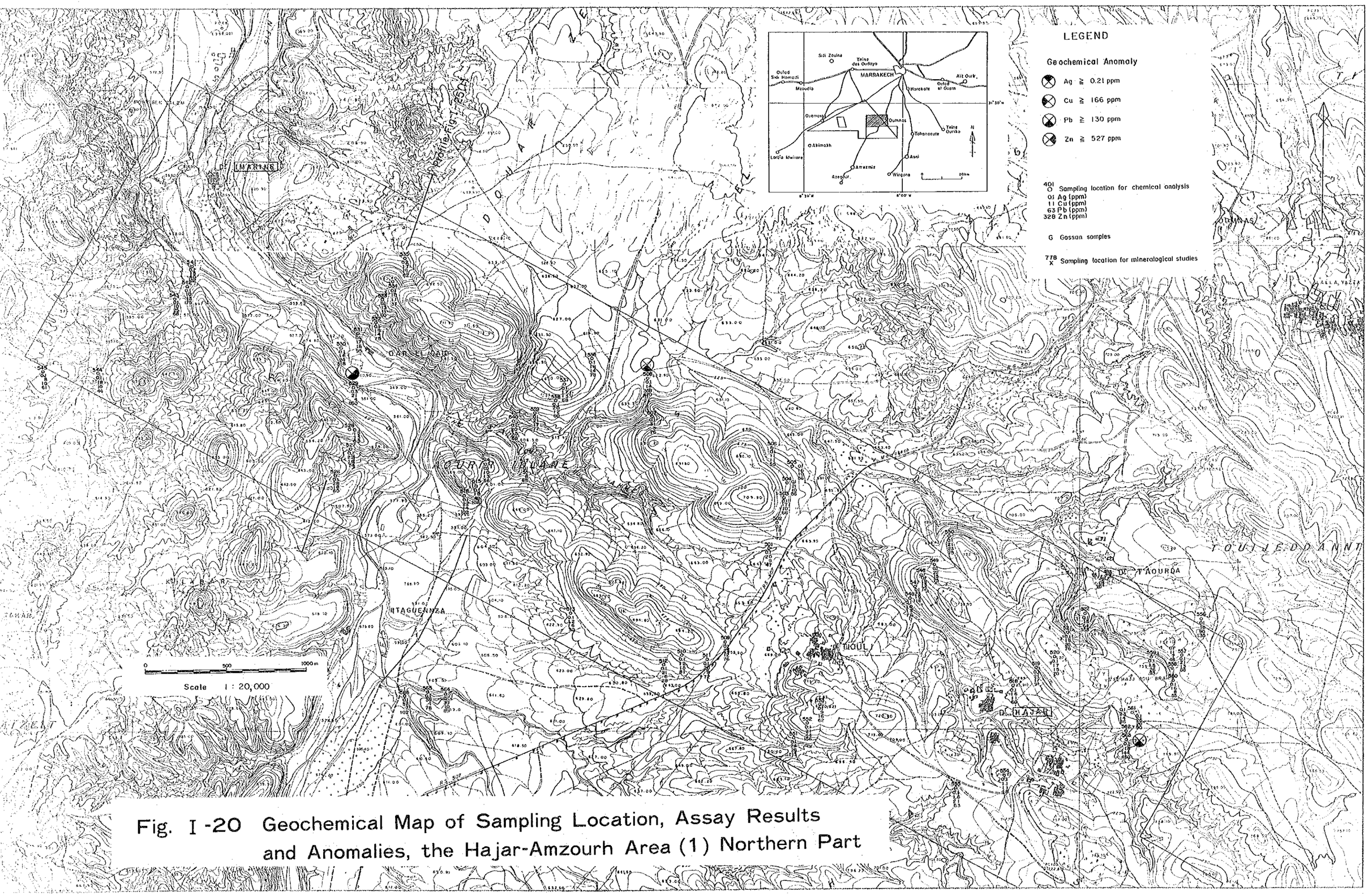

Fig. I-20 Geochemical Map of Sampling Location, Assay Results and Anomalies, the Hajar-Amzourh Area (1) Northern Part

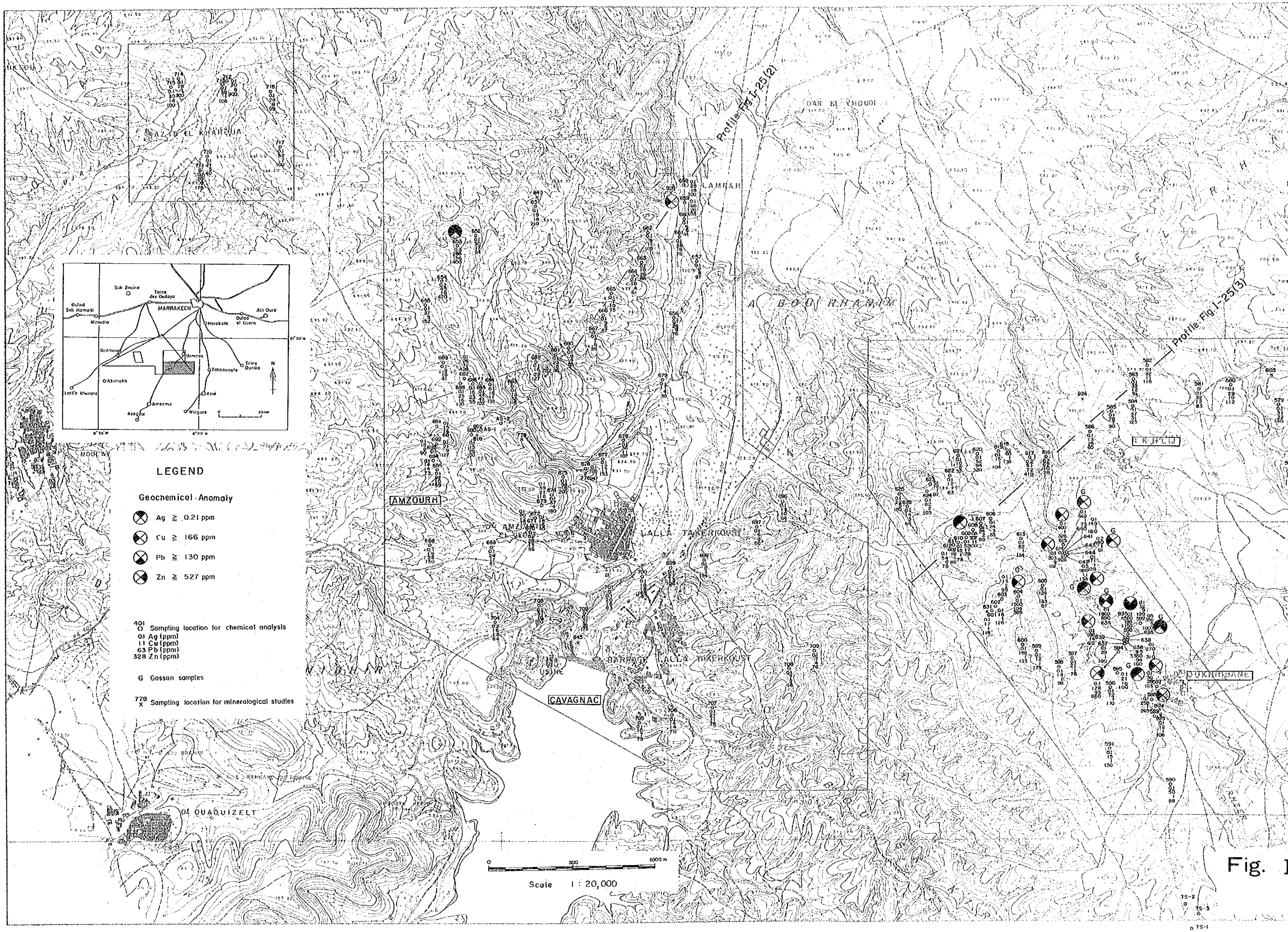

LEGEND
Geochemical · Anomaly
Ag ≧ 0.21 ppm
Cu ≧ 166 ppm
Pb ≧ 130 ppm
Zn ≧ 527 ppm
401 Sampling location for chemical analysis
01 Ag (ppm)
11 Cu (ppm)
63 Pb (ppm)
328 Zn (ppm)
G Gossan samples
778 x Sampling location for mineralogical studies
MARRAKECH
Sidi Zouine
Oulad Sidi Hamoti
Mzoudia
Ait Ourir
Oulad el Guern
Marekate
Tahanaoute
Amizmiz
Azegour
Asni
Wirgane
Lalla Takerkoust
AMZOURH
LALLA TAKERKOUST
BARRAGE LALLA TAKERKOUST
USINE
CAVAGNAC
LAMRAH
DAR EL YHOUDI
Profile Fig.I-25(2)
Profile Fig.I-25(3)
OUKHRBANE
Scale 1 : 20,000
0 500 1000 m
TS-2
TS-3
TS-1

Fig. I

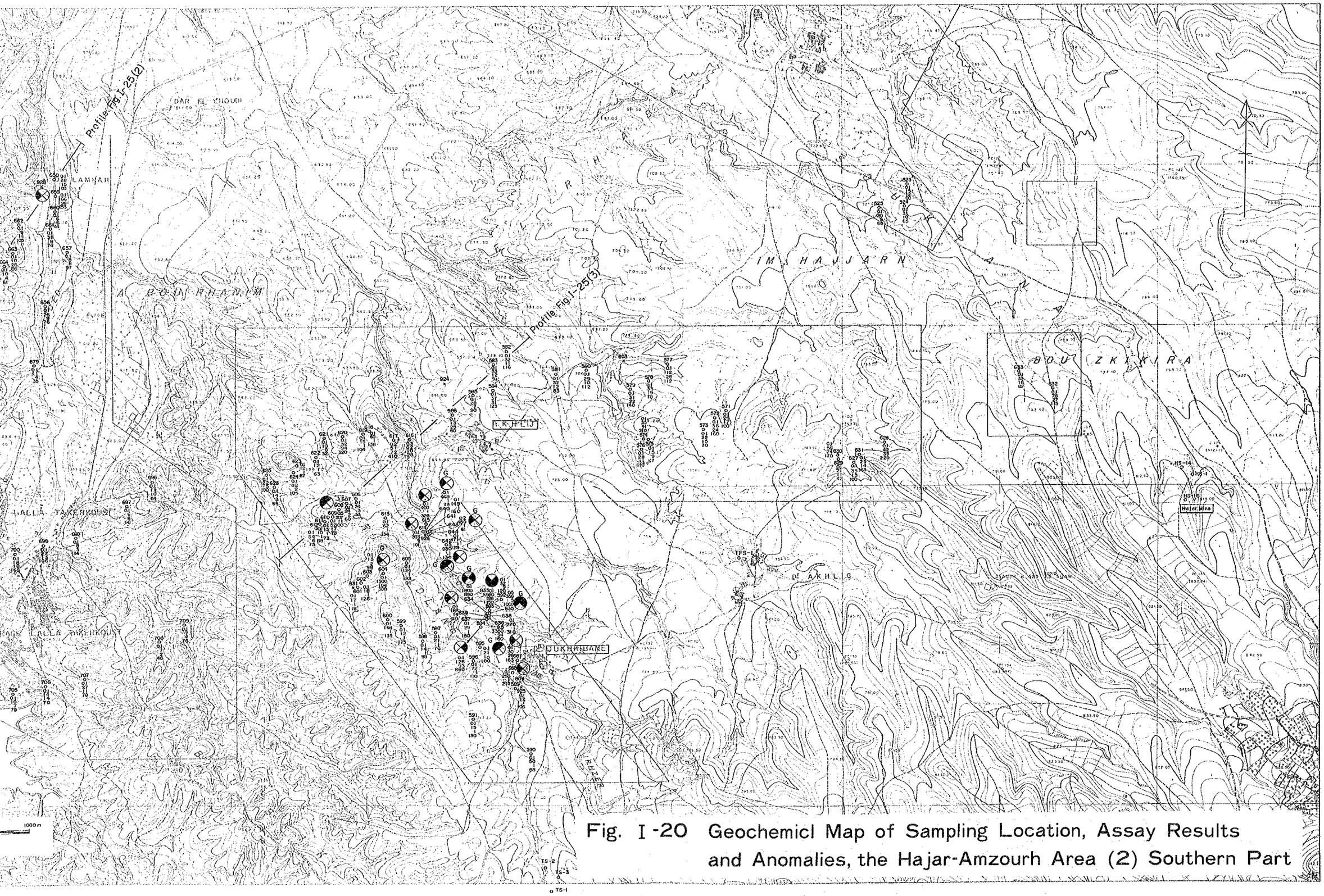

Fig. I-20 Geochemicl Map of Sampling Location, Assay Results and Anomalies, the Hajar-Amzourh Area (2) Southern Part

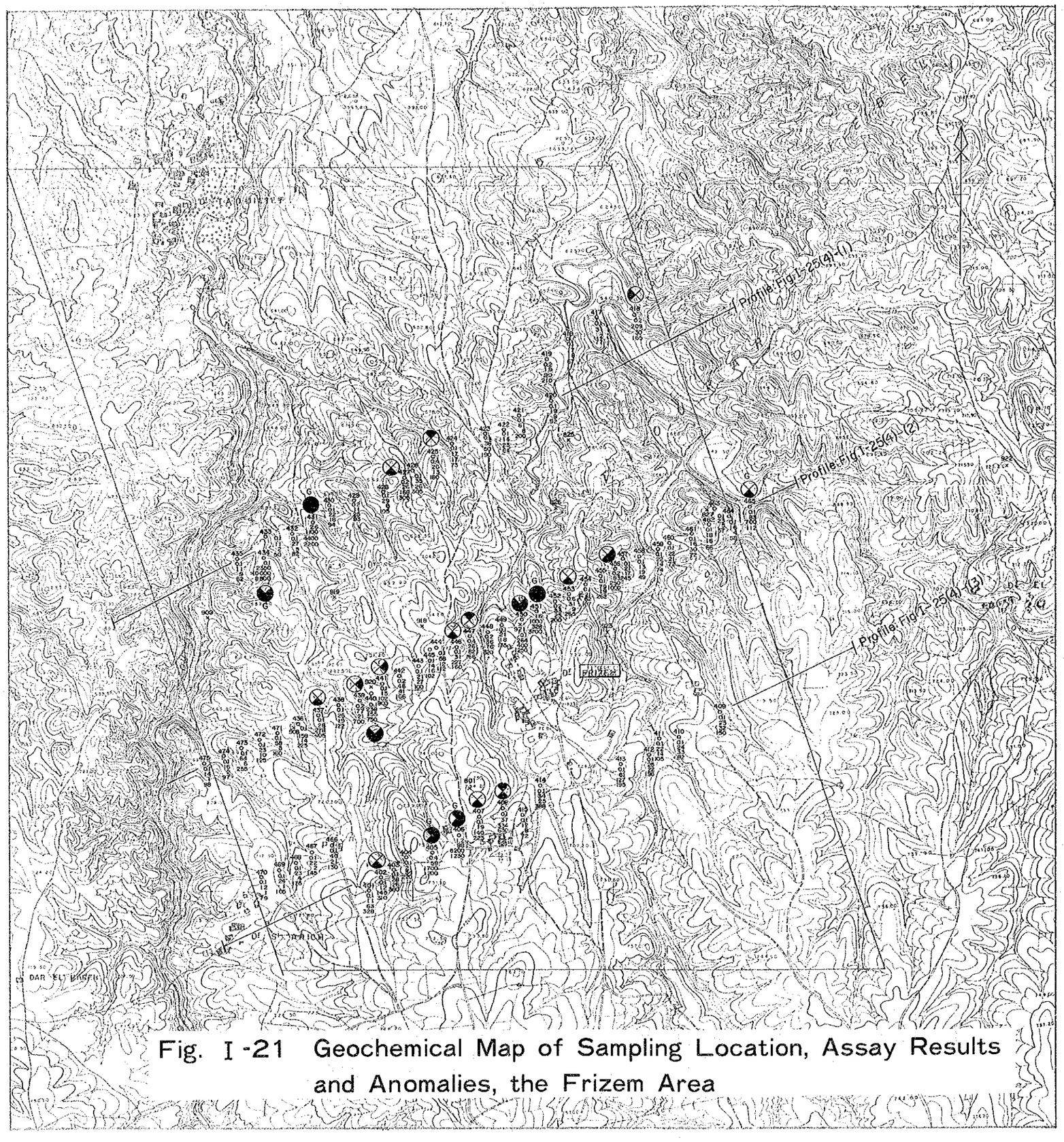

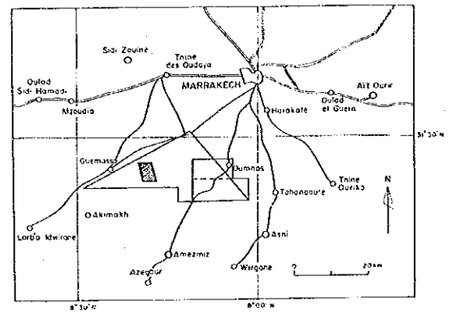

0 500 1000m

Scale 1 : 20,000

LEGEND

Geochemical Anomaly

- Ag ≧ 0.21 ppm
- Cu ≧ 166 ppm
- Pb ≧ 130 ppm
- Zn ≧ 527 ppm

401 O Sampling location for chemical analysis
01 Ag (ppm)
11 Cu (ppm)
63 Pb (ppm)
328 Zn (ppm)

G Gossan samples

778 X Sampling location for mineralogical studies

Fig. I-21 Geochemical Map of Sampling Location, Assay Results and Anomalies, the Frizem Area

Pb—Cu

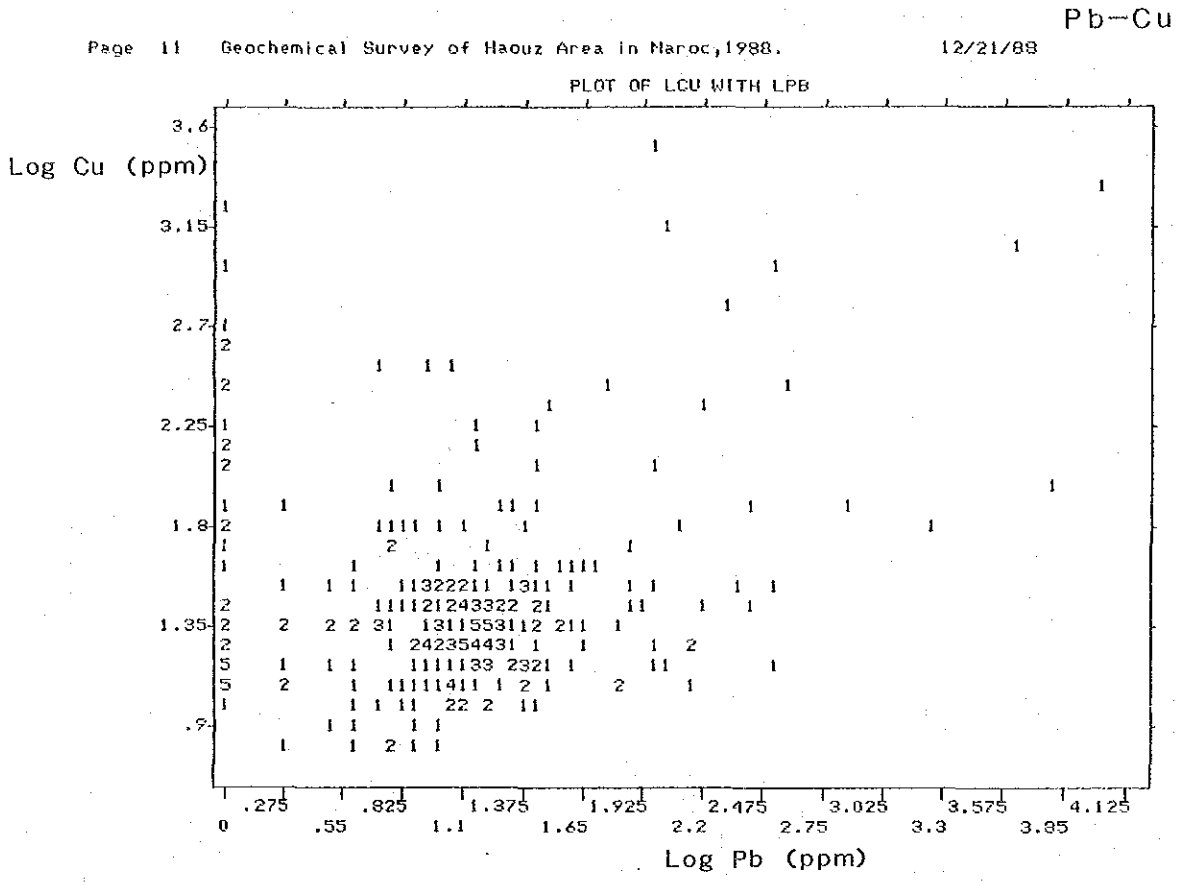

Zn—Cu

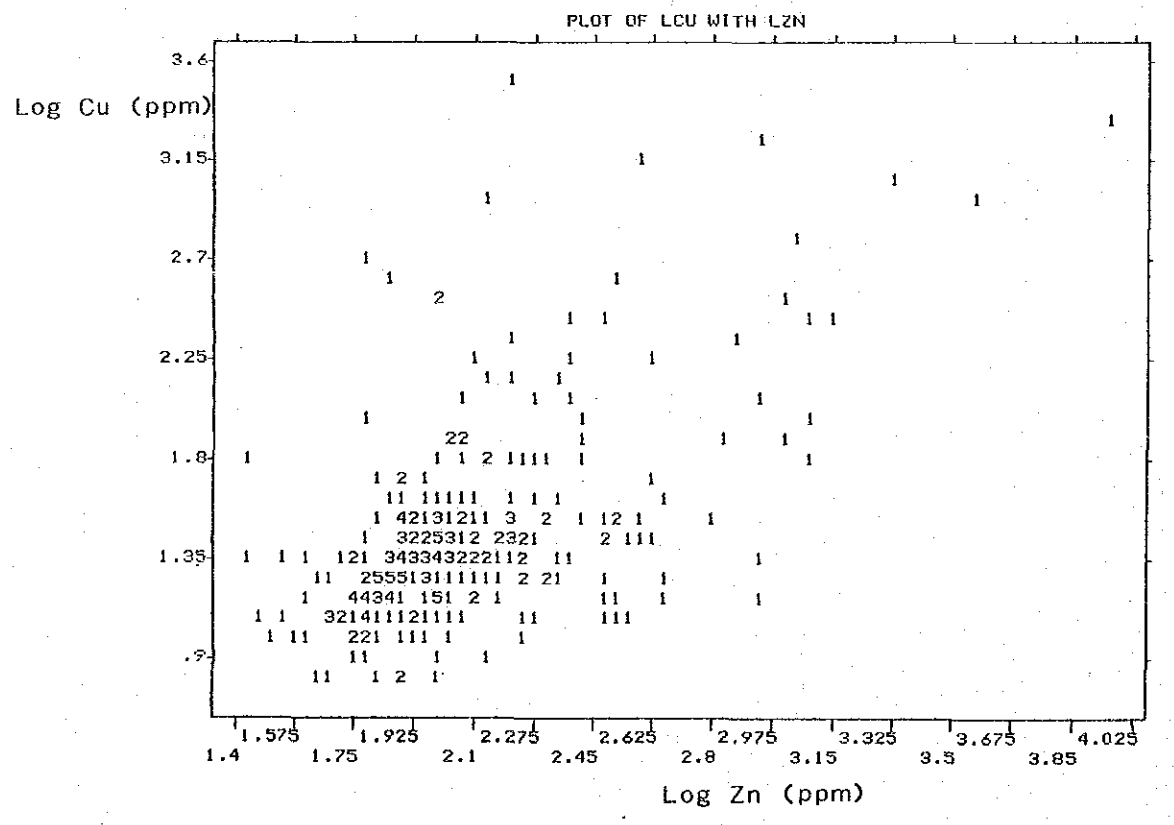

Fig. I—22 Dispersion Diagram of Geochemistry (1)

Ag—Cu

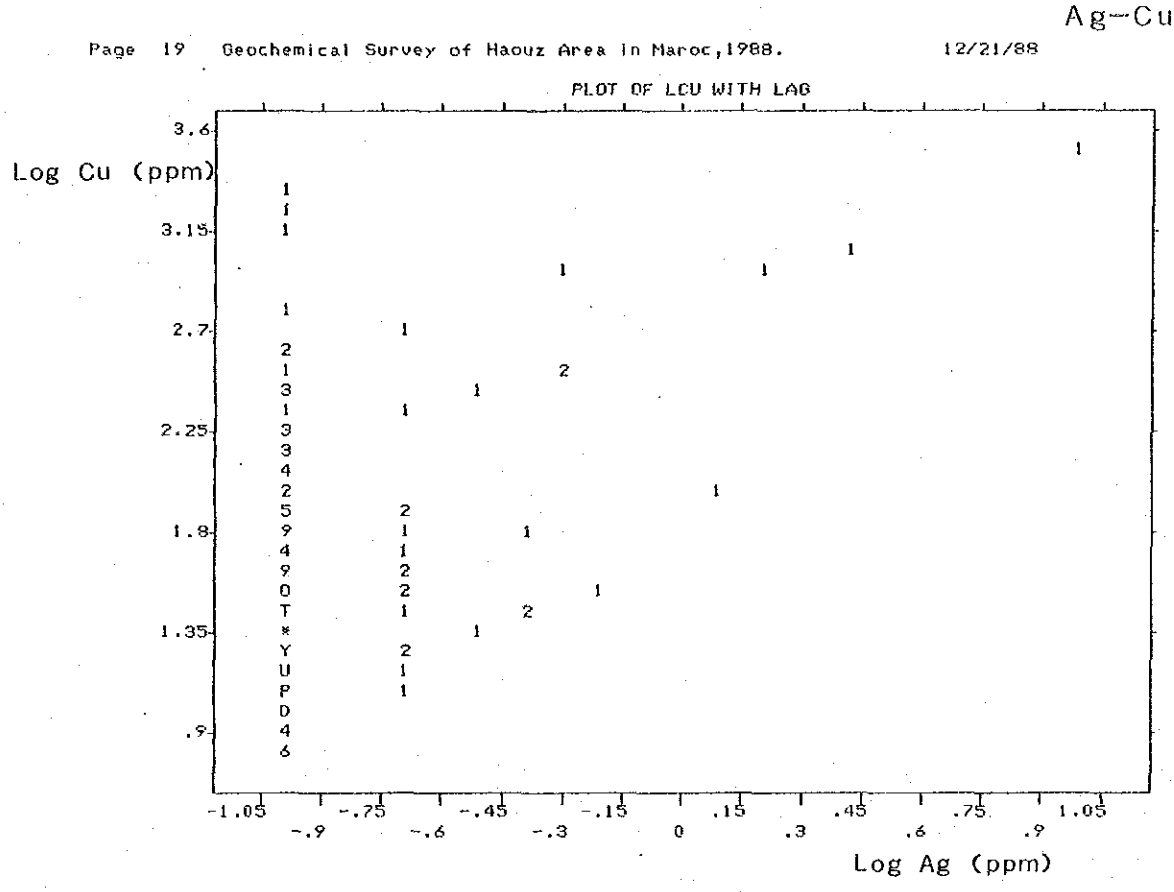

Zn—Pb

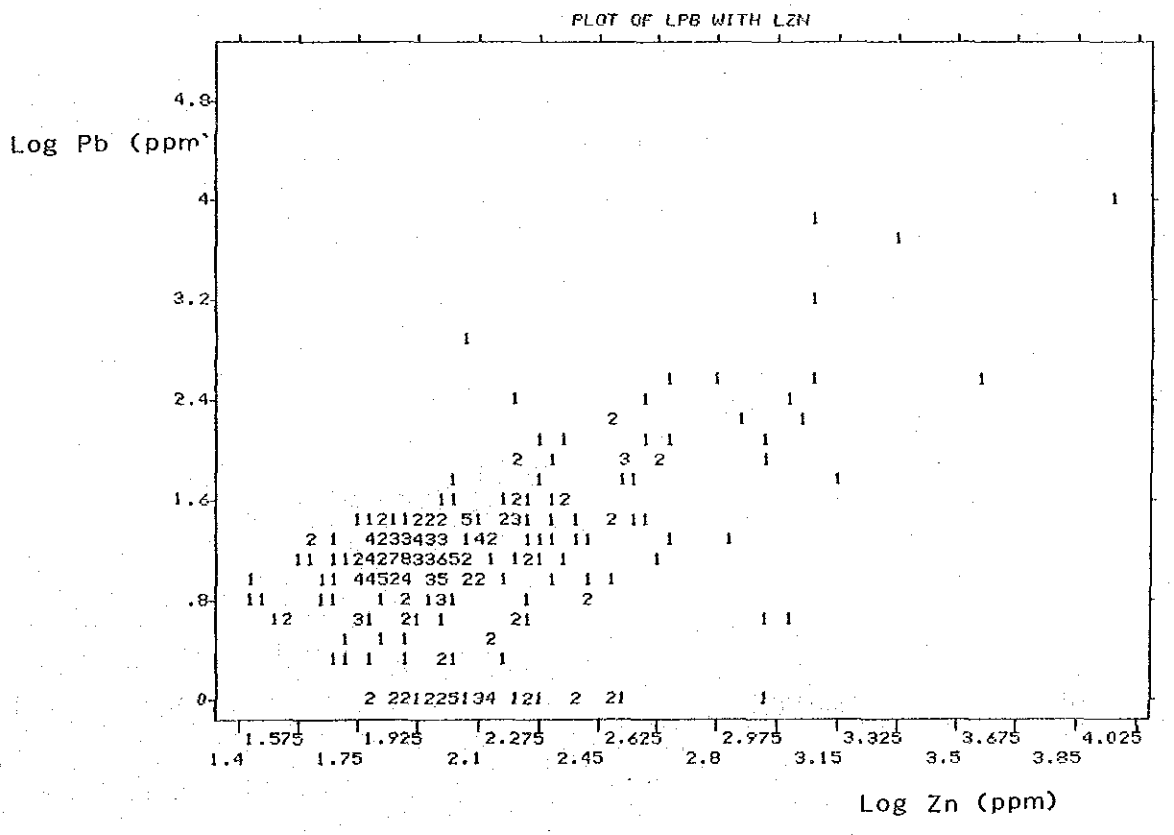

Fig. I—22 Dispersion Diagram of Geochemistry (2)

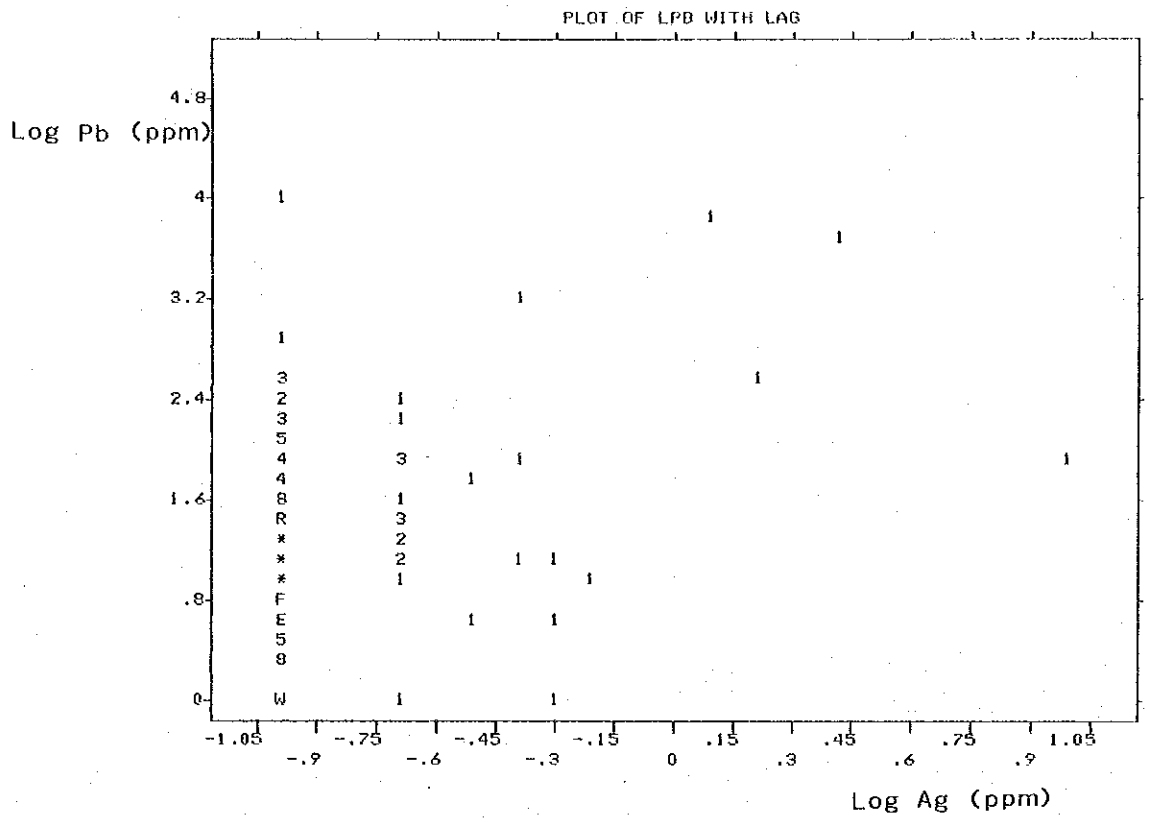

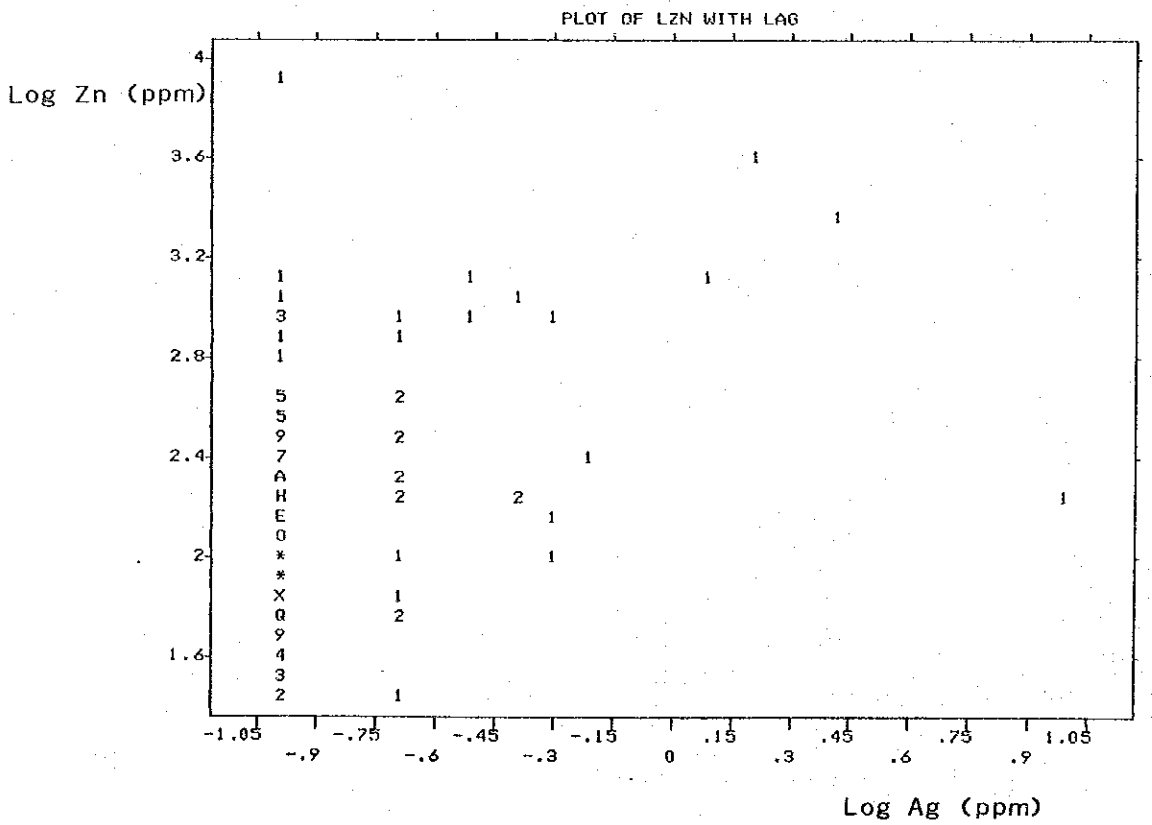

Fig. I—22 Dispersion Diagram of Geochemistry (3)

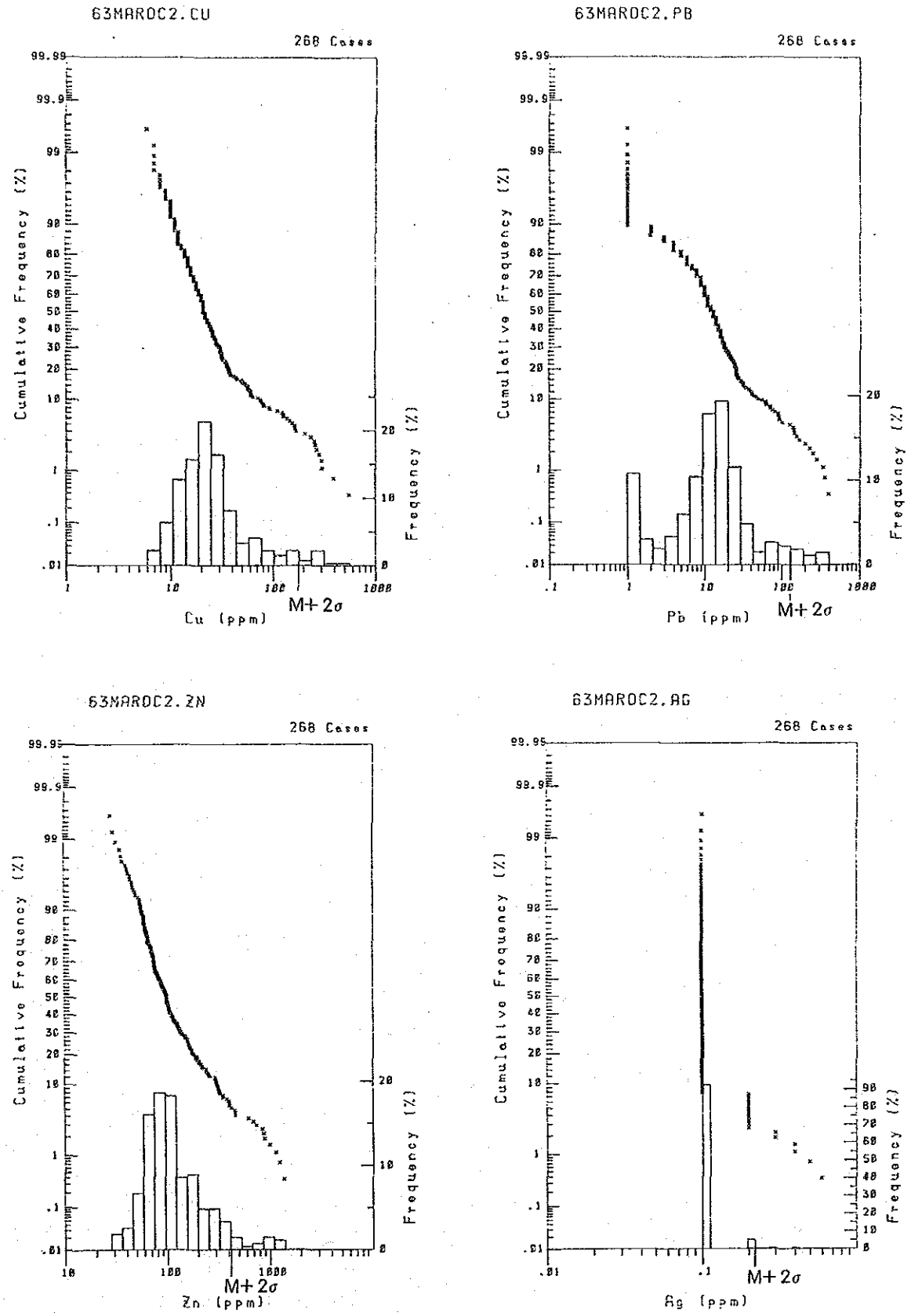

Fig. I—23 Histogram and Cumulative Frequency Curve of Geochemistry

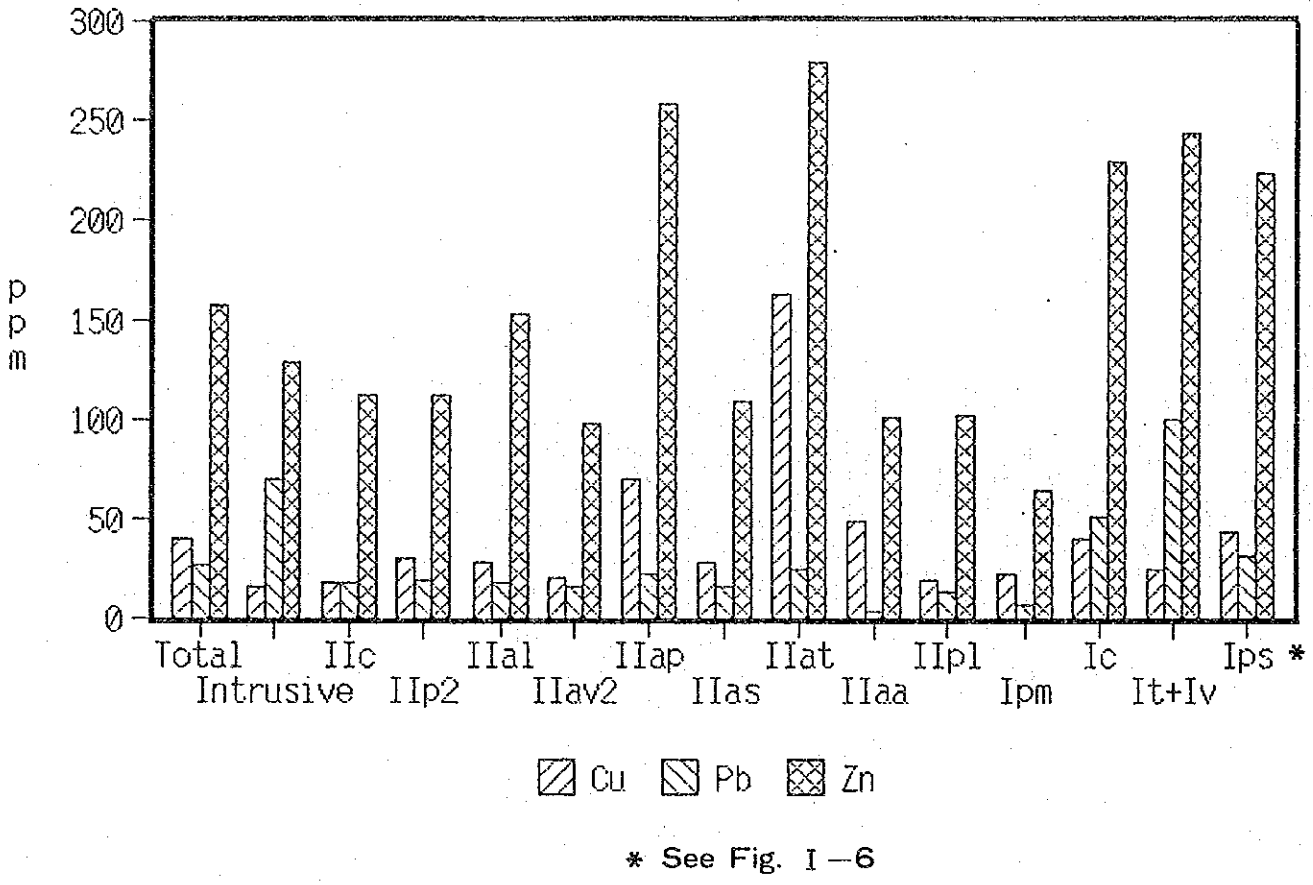

* See Fig. I—6

Fig. I—24 Geometric Means of Geochemistry, Classified by Each Geologic Unit

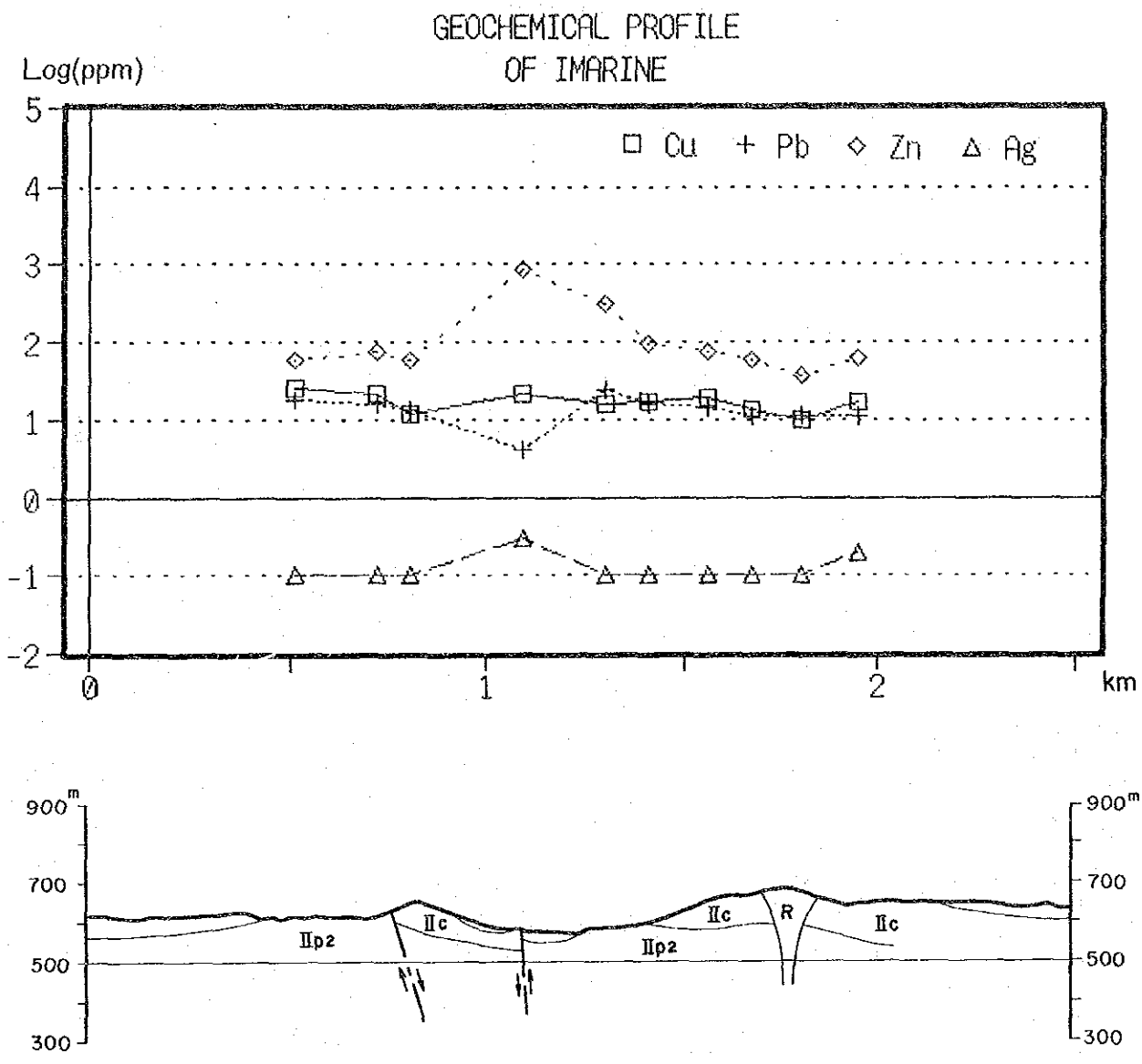

Fig. I-25 Geochemical Profile (I) Imarine Area

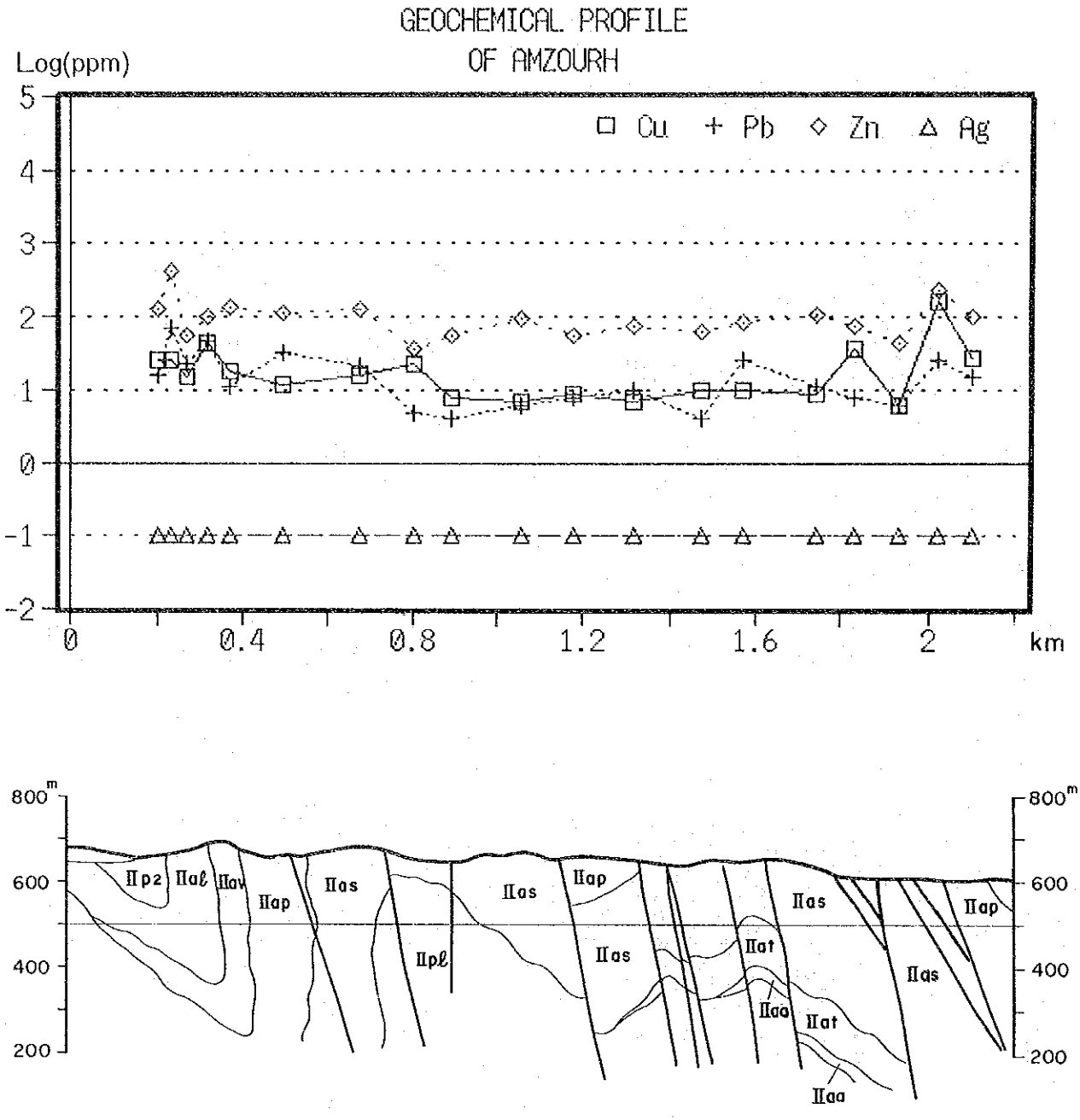

Fig. I-25 Geochemical Profile(2) Amzourh Area

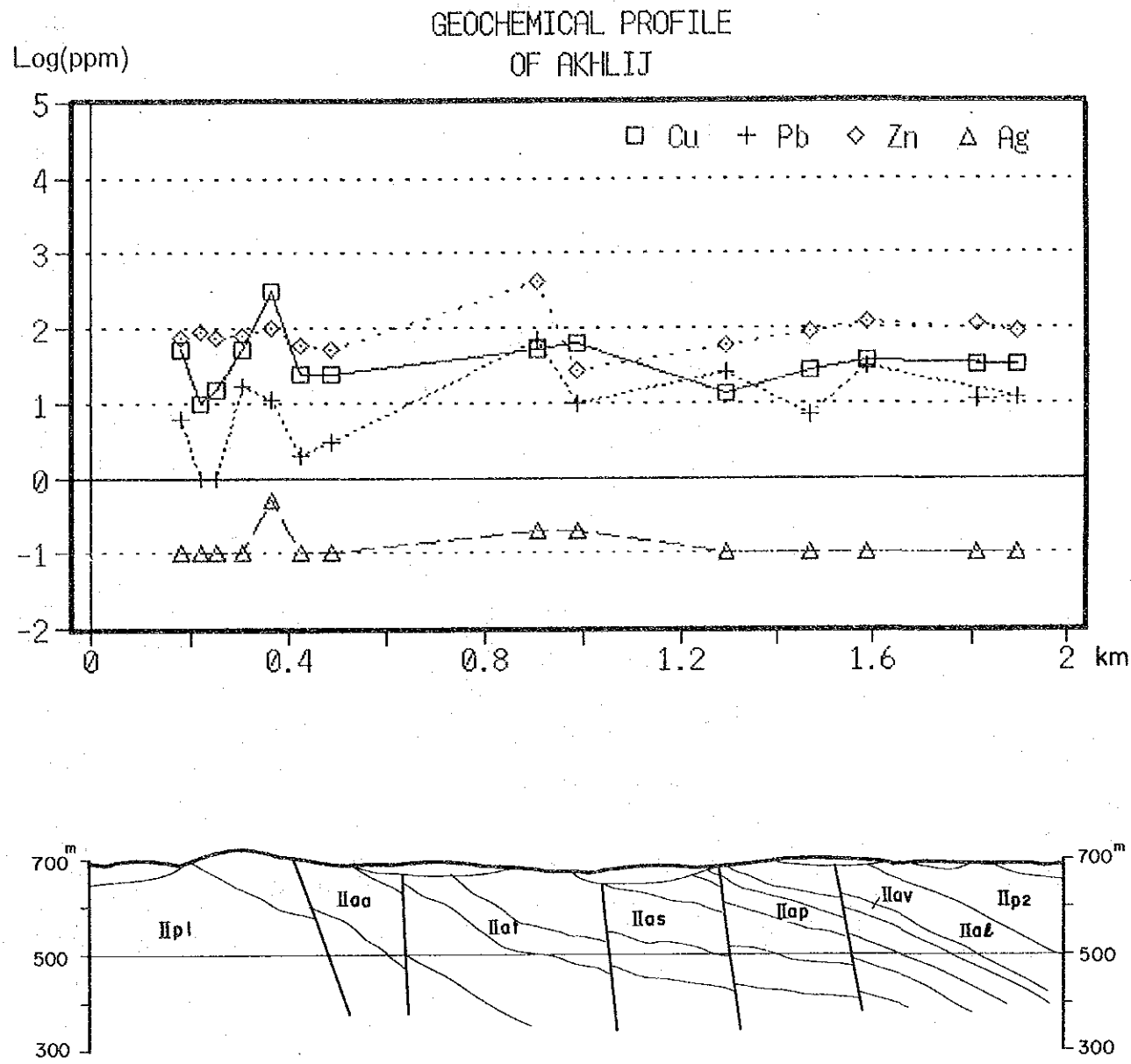

Fig. I-25 Geochemical Profile(3) Akhlij Area

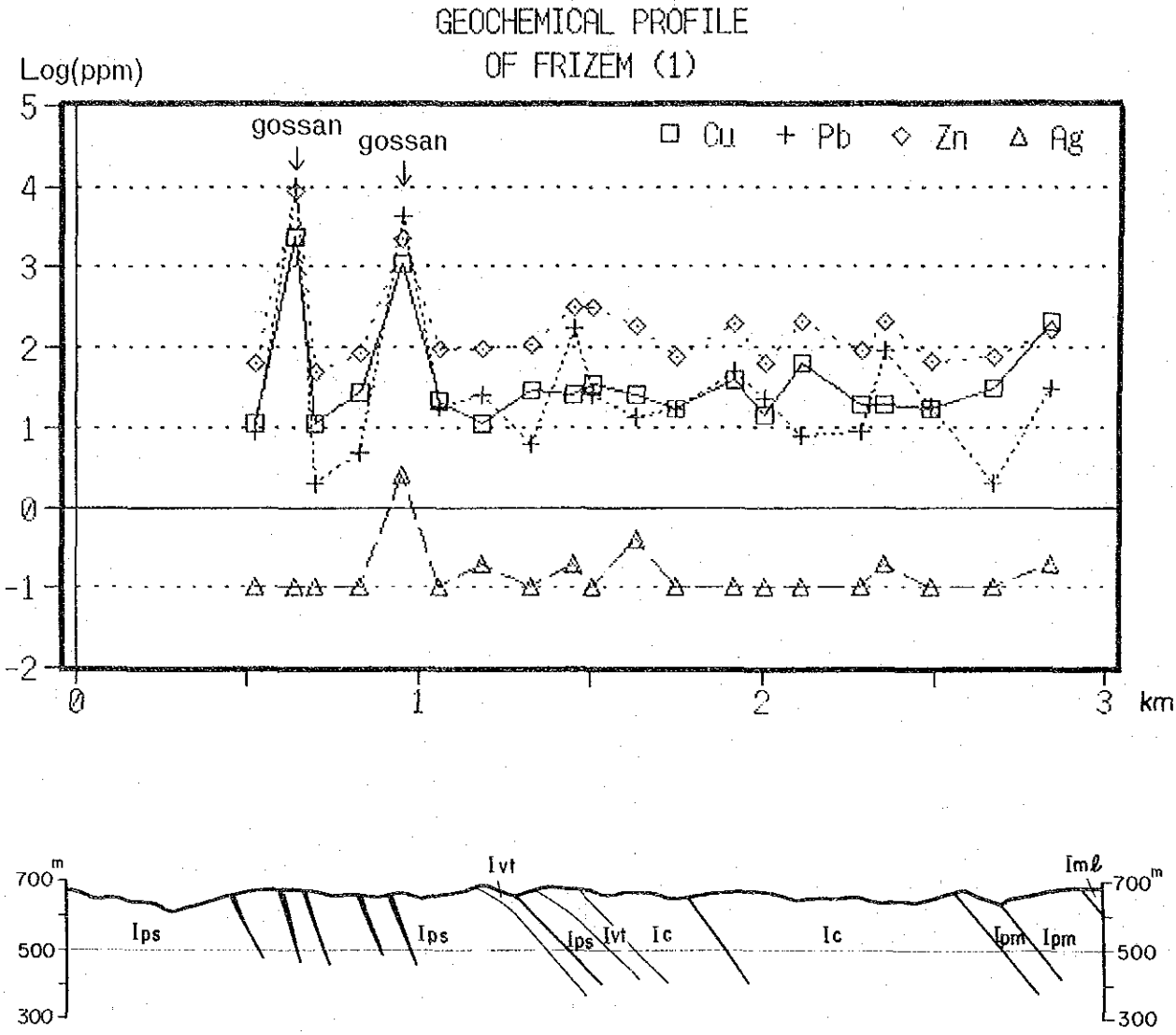

Fig. I-25 Geochemical Profile (4) Frizem Area (I)

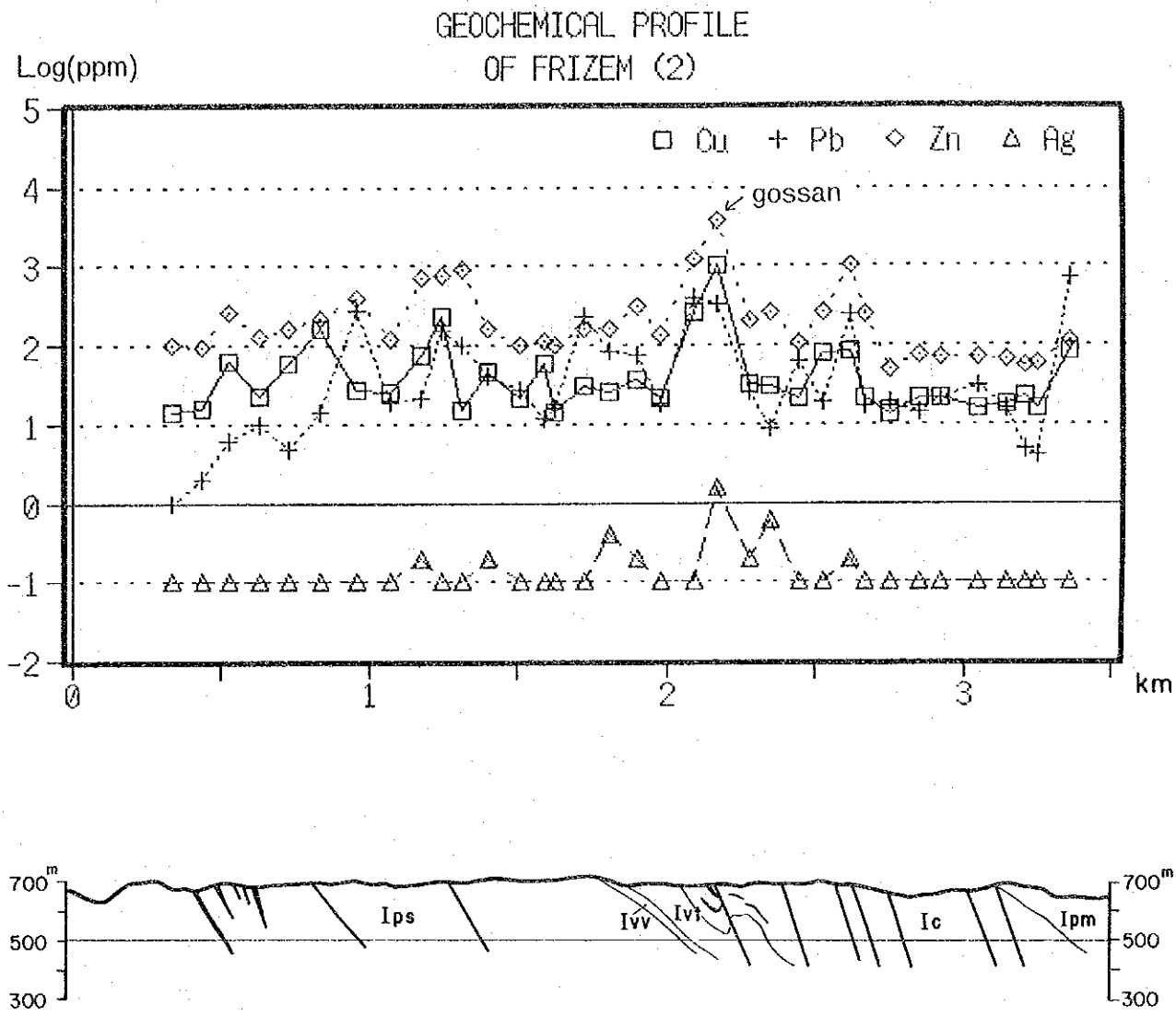

Fig. I-25 Geochemical Profile (4) Frizem Area (2)

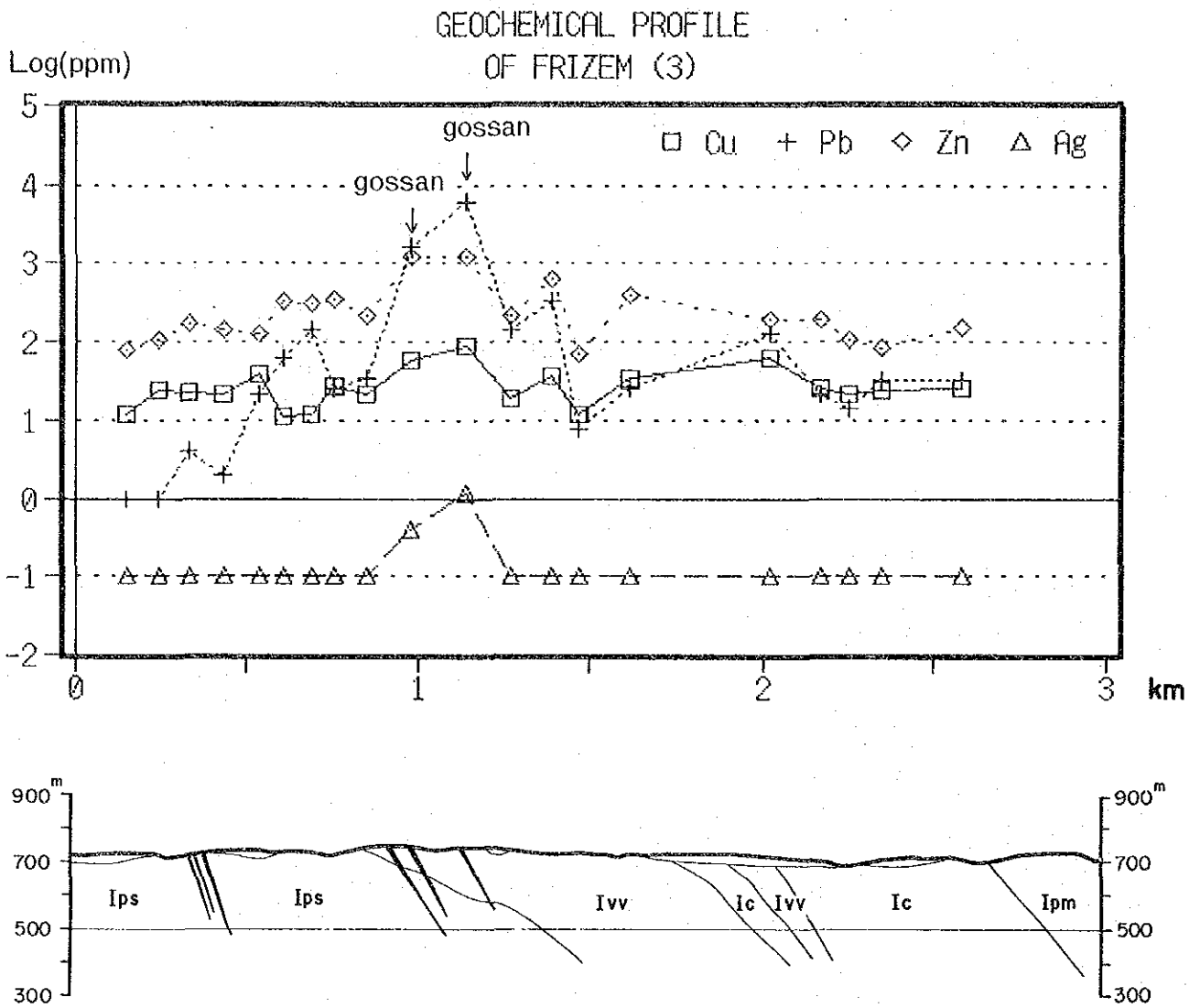

Fig. I-25 Geochemical Profile (4) Frizem Area (3)

Tab. I -1 List of Mineralized Zones

No	Name	Type of Indication	Location	Commodity	Shape of Ore body	Type of Mineralization	Host Rock		Scale of Ore body (m)	Scale of Zone (m)	Strike and Dip	Grade of Ore	Ore Mineral	Gangue Mineral	Remarks
							Fm.*	Rock							
1	Hajar Deposit	Magnetic Anomaly	Hajar	Cu Pb Zn Ag	massive	sedimentary	Ⅱat	Tuff	100×400 ×500	+500	NW-SE, 50° NE	Ag= 74ppm Cu= 0.86 % Pb= 2.78 % Zn= 9.45 %	Cp·Gl Sp·Po Py	Qt·Talc Chl·Ser Cal	DDH = 27holes Shaft= 235 m Adit = 293 m
2	Oukhribane-E	Gossan	Oukhribane	Cu Zn	network	fissure-filling	Ⅱat	Tuff	20×60	+100	NW-SE, 80° NE	Ag= 0.3ppm Cu= 0.06 % Pb= tr Zn= 0.0 1%	Hm·Ge	Qt	
3	Oukhribane-W	Gossan	Akhlij	Cu Zn	network	fissure-filling	Ⅱat	Tuff	20×70	+100	WNW-ESE 80° NE	Ag= 0.3ppm Cu= 0.06 % Pb= tr Zn= 0.01 %	Hm·Ge	Qt	
4	Tiferouine	Magnetic Anomaly	3km S from Akhlij	Cu	dissemination	replace	Ⅱp	Slate	20				Cp·Py Mg·Po	Qt	DDH = 3holes
5	Tifratine		Akhlig	Pb Zn	dissemination	sedimentary	Ⅱat	Tuff	7			Ag= 7ppm Cu= 0.01 % Pb= 0.2 % Zn= 0.6 %	Sp·Po	Qt	DDH = 1hole
6	Amzourh	Gossan	Amzourh	Cu Pb Zn	dissemination	fissure-filling	Ⅱav	Volcanic Rock	2×20	+500	NW-SW 80° NE	Ag= 8ppm Cu= 0.85 % Pb= 1.77 % Zn= 1.17 %	Hm·Ge Cu-Ox	Qt·Cal	DDH = 2holes
7	Frizem-E	Gossan	Frizem	Cu Pb Zn	dissemination	sedimentary replace	Ⅰc	Marl Slate	10×40	+500	NNW-SSE 30° E	Ag= 15ppm Cu= 0.36 % Pb= 0.63 % Zn= 1.76 %	Cp·Gl Sp·Py Po	Sid·Qt Cal	DDH = 9holes
8	Frizem-W	Gossan	Frizem	Cu Pb Zn	dissemination	fissure-filling	Ⅰps	Slate	2×50	+700	NNW-SSE 50° E	Ag= 5ppm Cu= 2.25 % Pb= 0.61 % Zn= 1.63 %	Hm·Ge Cu-Ox	Qt·Sid Cal	DDH = 1hole
9	Mjed	Gossan	6km E from Frizem		dissemination	replace	Ⅰl	Limestone	2×50	+300	NNW-SS E 80° E	Ag= 1ppm Cu= tr Pb= tr Zn= 0.01 %	Hm·Ge Po	Sid·Qt	DDH = 1hole

Cp : Chalcopyrite
Gl : Galena
Sp : Sphalerite
Po : Pyrrhotite
Py : Pyrite

Mg : Magnetite
Hm : Hematite
Ge : Goethite
Ox : Oxide

Qt : Quartz
Chl: Chlorite
Ser: Sericite
Cal: Calcite
Sid: Siderite

* See Fig. I - 6.

Tab. I-2 Statistical Values of Geochemical Assay Results

Geologic Unit *1	No. of Samples	Cu (ppm)				Pb (ppm)				Zn (ppm)				Ag (ppm)			
		Mean	Std	Min	Max	Mean	Std	Min	Max	Mean	Std	Min	Max	Mean	Std	Min	Max
Total *2	268	40.15	62.74	6	560	26.49	51.87	1	400	157.11	184.88	28	1400	0.11	0.05	0.1	0.6
Intrusive	6	15.33	7.92	10	31	69.33	141.63	3	358	128.67	168.51	37	470	0.10	0.00	0.1	0.1
IIc	38	17.68	4.75	9	31	18.00	15.88	4	90	111.58	144.11	44	880	0.11	0.04	0.1	0.3
IIp2	37	29.70	18.26	8	112	19.19	22.84	4	144	111.62	79.08	28	460	0.10	0.00	0.1	0.1
IIal	22	27.64	14.36	9	76	17.18	16.69	1	71	152.59	119.74	41	470	0.10	0.02	0.1	0.2
IIav	7	19.86	9.86	10	37	15.29	8.88	4	28	97.43	37.35	60	160	0.11	0.04	0.1	0.2
IIap	11	69.27	85.61	9	288	21.82	15.18	6	56	258.09	384.18	57	1400	0.12	0.06	0.1	0.3
IIas	24	28.00	30.50	6	128	15.04	22.06	1	94	108.54	95.14	28	410	0.11	0.03	0.1	0.2
IIat	16	162.31	160.12	8	560	24.06	51.63	1	198	278.88	304.40	76	1150	0.10	0.00	0.1	0.1
IIaa	23	48.78	67.32	10	307	2.83	3.88	1	17	100.30	34.31	53	183	0.12	0.08	0.1	0.5
IIpl	15	19.33	9.69	6	36	13.33	9.24	2	38	101.87	38.49	46	173	0.10	0.00	0.1	0.1
Iml	1	209.00	0.00	209	209	30.00	0.00	30	30	165.00	0.00	165	165	0.20	0.00	0.2	0.2
Ipm	4	22.00	6.68	16	31	6.75	6.29	2	16	64.50	9.26	57	77	0.10	0.00	0.1	0.1
Ic	24	39.46	51.35	13	264	50.88	89.20	8	400	229.58	288.38	49	1250	0.15	0.12	0.1	0.6
Ivt+Ivv	15	24.80	13.62	11	61	99.20	92.57	8	334	243.27	144.31	72	630	0.14	0.08	0.1	0.4
Ips	25	43.64	50.98	11	238	31.52	61.98	1	278	224.08	229.17	50	900	0.11	0.03	0.1	0.2

(Samples are rocks and gossans)

Mean : Geometric Mean
Std : Standard Deviation
Min : Minimum
Max : Maximum

*1 See Fig. I - 6.
*2 exclude gossan samples

Tab. I-3 List of Anomalous Geochemical Rock Samples

Area	No.	Unit*	Grade (ppm)			
			Cu	Pb	Zn	Ag
Frizem	402	Ivv	12	145	310	0.1
	407	Ivv	19	140	225	0.1
	408	Ivv	37	334	630	0.1
	416	Iml	209	30	165	0.2
	425	Ic	26	13	180	0.4
	427	Ivt	26	168	305	0.2
	437	Ips	28	278	405	0.1
	439	Ips	77	21	700	0.2
	440	Ips	238	155	750	0.1
	441	Ips	15	102	900	0.1
	446	Ivv	31	227	160	0.1
	447	Ivv	26	82	166	0.4
	450	Ic	264	400	1250	0.1
	453	Ic	31	9	265	0.6
	456	Ic	83	250	1000	0.2
Imarine	508	Dk	14	358	470	0.1
	529	IIc	21	4	880	0.3
	563	IIp2	18	144	460	0.1
Oukhribane	588	IIat	258	1	245	0.1
	593	IIat	560	198	1150	0.1
	594	IIat	128	93	860	0.1
	608	IIaa	307	11	100	0.5
	614	IIat	303	9	101	0.1
	615	IIat	400	1	326	0.1
	638	IIat	270	1	310	0.1
	639	IIat	166	14	410	0.1
	644	IIat	171	1	128	0.1
Amzourh	653	IIap	288	56	1400	0.3
	659	IIap	166	26	233	0.1

* See Fig. I - 6. (Samples are rocks)

Tab. I-4 List of Gossan Samples

Area	No.	Grade (ppm)			
		Cu	Pb	Zn	Ag
Frizem	405	58	1700	1200	0.4
	406	88	6200	1230	1.2
	431	1100	4400	2200	2.6
	434	2350	10000	8800	0.1
	451	1000	328	3700	1.6
	465	83	700	112	0.1
Oukhribane	604	1500	104	388	0.1
	634	1800	1	890	0.1
	635	356	5	1000	0.5
	636	3350	94	160	9.5
	637	29	1	180	0.1
	640	448	1	73	0.1
	642	980	1	134	0.5
	643	480	1	61	0.2

Tab. I-5 Dating Result by K-Ar method

Sample No.	Rock Type (Formation)*	Area	Material Analyzed	Isotopic Age (Ma)	$^{40}Ar^{*}$ (scc/gm$\times 10^{-5}$)	$\%^{40}Ar^{*}$	%K
801	Ryolite (Ivv)	Frizem	Whole rock	328. ±16.	3.63 3.61	97.5 98.3	2.58 2.59
802	Ryolite (I_{lav_2})	Amzourh	Whole rock	303. ±15.	.858 .850	91.7 91.6	.67 .66
803	Ryolite (I_{lav_2})	Akhlij	Whole rock	294. ±15.	2.80 2.99	96.5 98.0	2.33 2.33
804	Green Tuff (Ilat)	Oukhribane	Whole rock	297. ±15.	3.91 4.00	97.9 98.0	3.14 3.16

(by Teledyne Isotopes, USA)

$$T=1804.08\times \log_e \{(^{40}Ar^{*}\div K\times 0.1426)+1\}$$

T = age in million years
K in weight percent natural potassium
$^{40}Ar^{*}$ in scc/gm$\times 10^{-5}$

CHAPTER 4 CONSIDERATION

4-1 Stratigraphy, Lithology and Geological Structure

The basement rocks composing the Haouz Central Area are the schists originated from marly-pelitic sediments with limestone and siltstone layers. These schists are correlated to the lower middle part of the Carboniferous of the Paleozoic Era, as Entroques is found in the limestone. (P. Huvalin, 1973).

The main constituent minerals of the schists are chlorite, sericite, quartz and calcite, and it is thought that the metamorphic grade of the schists is not so high. In the schists, numerous schistosity faults are well developed and the repetition of the complicated drag folds is remarkable. It is thought from the above facts that the metamorphism prevailed in this area was dynamic metamorphism deforming the strata.

4-2 Age Determination of the Acidic Volcanic Rocks

Age determination was applied by K-Ar method on the acidic volcanic rocks and related pyroclastic rock collected in the Frizem Area and in the Hajar-Amzourh Area, to confirm the period of the volcanic activity and the relation to the Pb-Zn-Cu mineralization.

The result is as shown in the Tab. 1-5.

Sample No.	Rock Type (Fm)	Area	Isotopic Age (Ma)
801	rhyolite (Ivv)	Frizem area	328 ± 16
802	rhyolite (IIav2)	Amzourh area	303 ± 15
803	rhyolite (IIav2)	Akhlij area	294 ± 15
804	tuff (IIat)	Oukhribane area	297 ± 15

Examining the above 4 isotopic ages geo-historically, it can be said that these isotopic ages are in good accord with the ages of the sedimentary rocks estimated by fossils, as the rhyolite collected in the Frizem Area is corresponding to the lower part of the Carboniferous while the rhyolite and pyroclastic rock in the Hajar-Amzourh Area are corresponding to the upper part of the Carboniferous.

These volcanic rocks are foliated and schistose after the dynamic metamorphism. However, by the microscopic observation, they preserve mineral assemblage and texture of the original rock comparatively well, having quartz phenocysts and bearing sericite. It is thought that little dispersion of argon gas by heat addition would have occurred through the period of the metamorphism. If we would take the hypothesis that the argon gas had been dispersed, we would have much younger isotopic age than the true value, and the result would be greatly inconsistent with the result suggested from the biostratigraphy.

The results of the age determination and geological survey are thought to support the following estimation.

1) The period of the volcanic activity is before the Carboniferous, which is in good coincidence with the period of the sedimentation of the sedimentary rocks.

2) By the result of the First Phase surveys including the stratigraphical and tectonic studies, the volcanic activity is assumed to have been two different successive periods. It has been reconfirmed that the volcanic activity recognized in the Frizem Area is older than that found in the Hajar-Amzourh Area.

3) The volcanic rocks are thought to have been derived from submarine volcanic activities. The period of the mineralization brought about with these volcanic rocks is coincident with the period of the accumula-

tion of the host sedimentary rocks.

4-3 Whole Rock Analysis

The results of whole rock analysis on 10 rock samples are shown in the Ap. I-3 and protted in the A_1-C-F_1 diagram, A_2-K-F_1 diagram, and A_3-F_2-M diagram as shown in the Fig. I-26.

The values of SiO_2 contents of the volcanic rocks in the Frizem and Akhlij areas (No. 801 and No. 803) are 76.80%, which are classified to rhyolite. The volcanic rock in the Amzourh area (No. 802) is of dacitic property as the contents of SiO_2 is 62%. The dolerite sample in the Frizem area (No. 825), which is dyke in the marly schist, has been replaced by calcite to the contents of 5.3% in CaO_2 contents.

In the A_1-C-F_1 diagram, the marlstone (No. 826) is rich in CaO_2 corresponding to the contents of 30% in $CaCO_3$. The taffceous green rocks inferred to be the host rock of ore deposit (No. 804, 813, 814, 831) are classified to the group that is poor in $CaCO_3$.

In the A_2-K-F_1 diagram, the dolerite (No. 825) is rich in the basic elements (FeO + MgO) and poor in the felsic elements (Al_2O_3 and K_2O). In the A_3-F-M diagram, a transitional series of the contents of MgO is found in the tuffaceous green rocks.

Generally speaking, the tuffaceous green rocks are rich in MgO and K_2O elements and characterized by extraordinal high ratio of K_2O/NaO.

4-4 Characteristics of the Hajar Ore Deposit

Fig. I-26 is the illustration showing the area occupied by the ore-bodies projected on the tunnel plan of -235 mL as shown in Fig. I-15. Neglecting small scale dislocation and deformation caused by the schistosity faults and drag folds, the general stratigraphical structure on

this level is taken to have the strike of N45°W and the dip of 40° - 50° to NE.

By preparing an illustration of the above plan inclined at 45° to the direction of S45°W and by projecting the geology and orebodies on this inclined plan onto the NW-SE section, an imaginative section as shown in Fig. I-26(B) is given as to the orebodies, which is thought to represent the original condition when they were formed, before the deformation and the dynamic metarmophism. Also, the general trend of the vein networks recognized at the bottom of the bedded orebodies is the combination of the two systems, which are represented by the trends of strike N25°E with dip of 30°E and of strike N25°W with dip of 30°W. Any by the same operation as above-mentioned, the strikes of the networks are approximately N25°E and N25°W and the dips are 70°E and 80°W, respectively.

This section is thought to represent the genetic model of the ore deposit. The form of the ore deposit is like a mushroom, the lamp-shade of which is representing the bedded orebody while the trunk is corresponding to the stockwork orebody with ore veins in the surrounding area.

The bedded orebody is composed not of a single layer, but of the repetition of several layers containing abundant pyrrhotite. In the intervals of these layers there are silicified rocks or talc-chlorite rocks. In the uppermost portion of the orebody, lead-zinc-silver concentration is recognized, where the highest assay result shows the ore grade of Pb 10%, An 20%, and Ag 200 g/t, though Cu grade is more or less 0.2%.

In the lower part of the orebody, lead and zinc contents are decreasing while the copper grade is comparatively increasing. The

average grade of the lower part is roughly Pb less than 5%, Zn less than 10%, Ag less than 50 g/t and Cu more or less 0.6%.

The stockworks and the ore veins are composed of pyrite-pyrrhotite-quartz veins containing zinc and copper. The average grade of the ore veins is Pb less than 1%, Zn less than 5%, Ag less than 10 g/t and Cu more or less 0.4%.

In the surrounding area of the ore deposit, distribution of fragmental ore transported and accumulated secondarily, is thought to be expected.

This model of mineralization is quite similar to the genetical model of Kuroko deposit presented by Tatsumi and Watanabe (1971), and Sato (1977), except for the difference of some points that the rock corresponding to the rhyolite lava dome of the Kuroko deposit is the pelitic-tuffaceous green rock in the Hajar deposit and that characteristic minerals of the Kuroko deposit such as barite and gypsum have not been recognized yet in the Hajar ore deposit.

The Hajar ore deposit has the following characteristics and is classified to be submarine exhalative sedimentary ore deposit.

1) The host rocks are marine sediments, and beneath the ore deposit, tuffaceous and pyroclastic dome is recognized, which is thought to have been formed by the submarine exhalation.

2) Main part of the ore deposit is bedded orebodies, at the bottom of which networks of veins are well developed.

3) The pelitic rocks overlying the ore deposit have not been influenced by the mineralization.

4-5 Characteristics of the Frizem Mineralization Zone

The east mineralization zone, which constitutes the main part of the Frizem mineralization zone, has the following characteristics and it is assumed that this mineralization zone would have been a sedimentary ore deposit formed at the marine floor.

1) The mineralization zone is distributed restrictedly in a certain horizon (marine sediments) overlying the acidic volcanics which is estimated to have been formed by the submarine exhalation.

2) The main part of the mineralization zone is composed of networks dissemination of ore minerals and typical bedded ore deposit has not been recognized, but the mineralized portions are remarkably brecciated, irregular in form, and discontinuous as to the distribution.

3) From the above characteristics, it is thought to be possible that the mineralization zone was formed through the secondary transportation and re-sedimentation, in addition to the influence of the deformation by the dynamic metamorphism.

The west mineralization zone is thought to have been formed in a series of mineralization in which the above-mentioned east mineralization zone was formed. It is assumed that the vein ore deposit in the pelitic rock underlying the acidic volcanic formation would have formed the mineralization zone by the deformation related to the dynamic metamorphism.

4-6 Genetic Model of the Ore Deposit

(1) Hajar Horizon

It is very difficult to describe the whole aspect of the Hajar horizon containing mineralization, as the exposure is quite sporadic and incomplete while various lithologic faces appear in the horizon.

By the integration and the consideration of the informations obtained through the present investigation, the details of the Hajar horizon and the relation of the horizon to the mineralization are shown in fig. I-28. As to the genesis of the Hajar ore deposit, the followings are assumed.

1) At the bottom of the quiet sea where the thick pelitic sediments were accumulated in the Carboniferous period, submarine volcanic activity occurred. Large amount of volcanic pyroclastic rocks and tuffs were exhalated, and a pyroclastic dome was formed at the central part of the activity.

2) The Hajar ore deposit was formed directly related to this submarine volcanic activity. Massive and bedded-type orebodies associated with Pb-Zn-Ag concentration were formed on the top or on the slope of the pyroclastic dome. Below that, stockwork-type orebodies containing Zn and Cu minerals were formed.

3) Through this volcanic activity, the sedimentary environment was changed great deal, and around the pyroclastic dome, contemporaneous heterotopic faces of the fine alternation of tuff and calcareous siltstone, the alternation of sandstone and mudstone, and tuffaceous mudstone were sedimented. At the bottom of the alternation of tuff and calcareous siltstone, there are lots of pebbles and nodules.

4) The submarine volcanic activity finished with the exhalation of rhyolite lava found in the Amzourh area, which formed small scale disse-

mination and vein ore deposit. In the quiet sea again, thick beds of limestone and mudstone were accumulated.

(2) Frizem Horizon

The types of the volcanic activity and the mineralization in the Frizem horizon are a little different from those in the Hajar horizon. A model section of the Frizem horizon is given in Fig. I-28(B).

1) Volcanic rocks formed by the volcanic activity in the Frizem horizon are composed mainly of rhyolite lava, which is similar to the volcanic activity in the Amzourh area.

2) The mineralization is related to the exhalation of the rhyolite, and has the characteristics of vein and replacement ore deposit formed at the bottom of the sea.

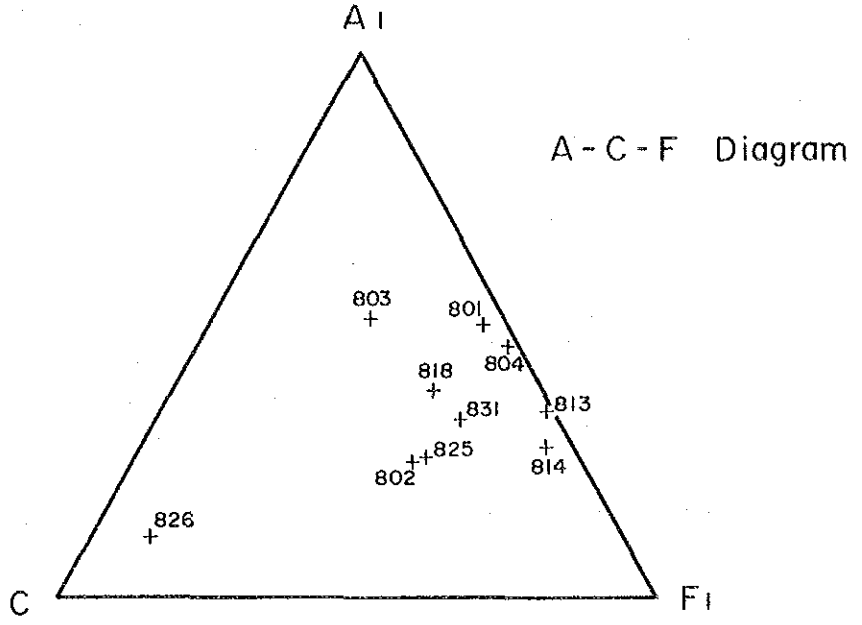

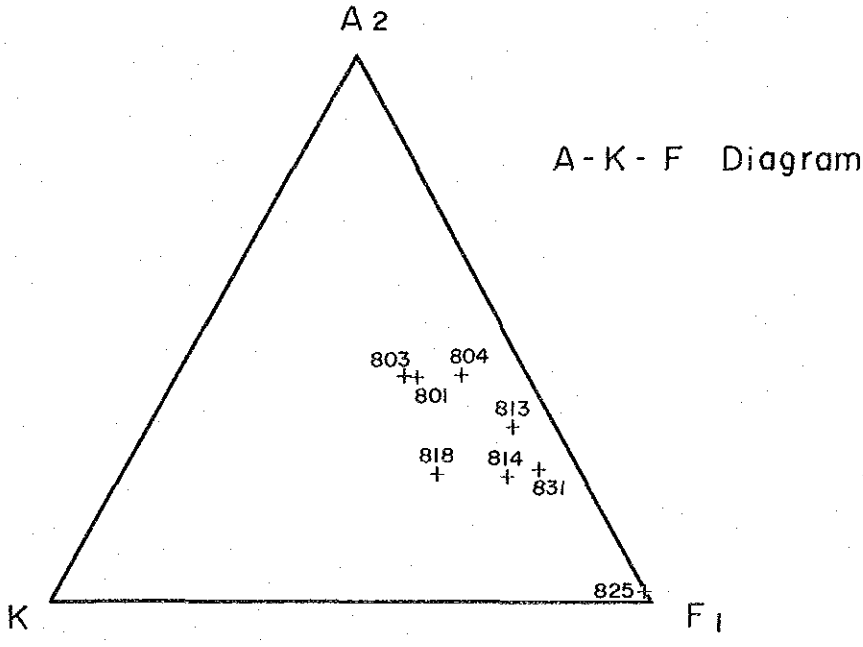

Fig. I - 26 Triangular Diagram for Rock Samples (I)

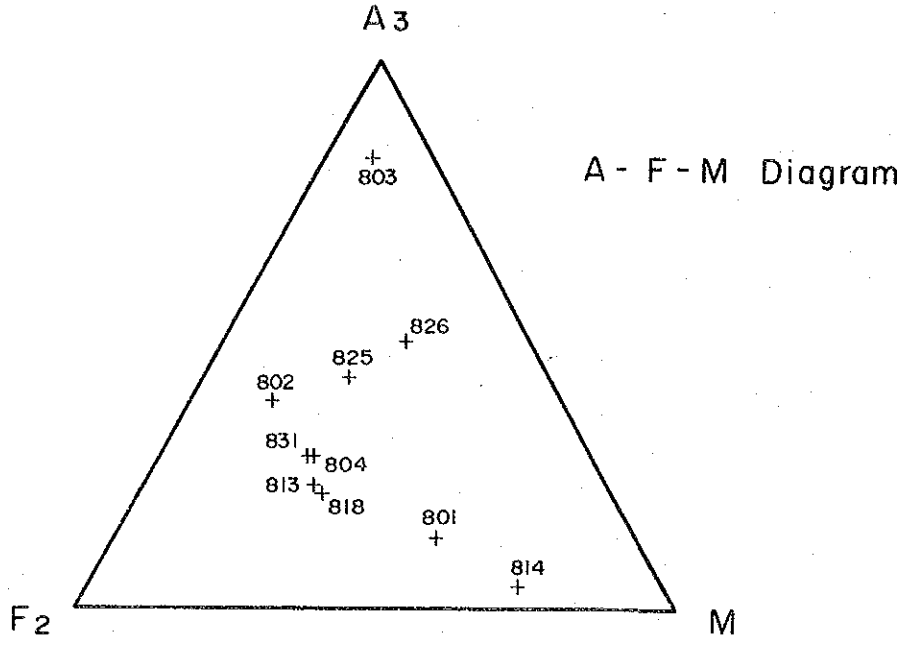

A - F - M Diagram

Sample No.	Rock Type
801	Ryolite
802	Ryolite
803	Ryolite
804	Pyroclastic Rock
813	Green Rock
814	Green Rock
818	Siltstone
825	Dolerite
826	Marl
831	Green Rock

$A_1 = Al_2O_3 + Fe_2O_3 - (Na_2O + K_2O)$, $C = CaO$, $F_1 = FeO + MgO + MnO$,
$A_2 = Al_2O_3 + Fe_2O_3 - (Na_2O + K_2O + CaO)$,
$A_3 = Al_2O_3 - 3K_2O$, $F_2 = FeO$, $M = MgO$

Fig. I - 26 Triangular Diagram for Rock Samples (2)

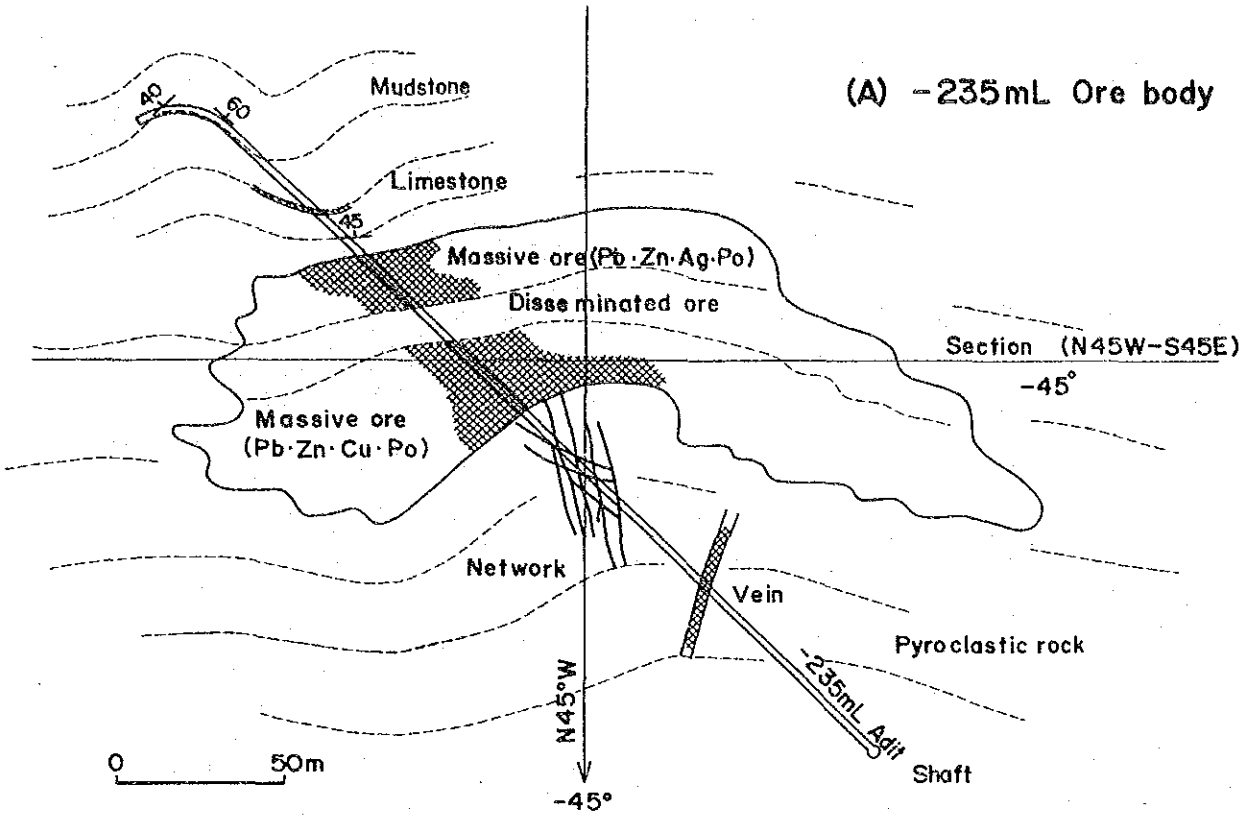

※ Shape of ore body was drawn using the surface drilling data

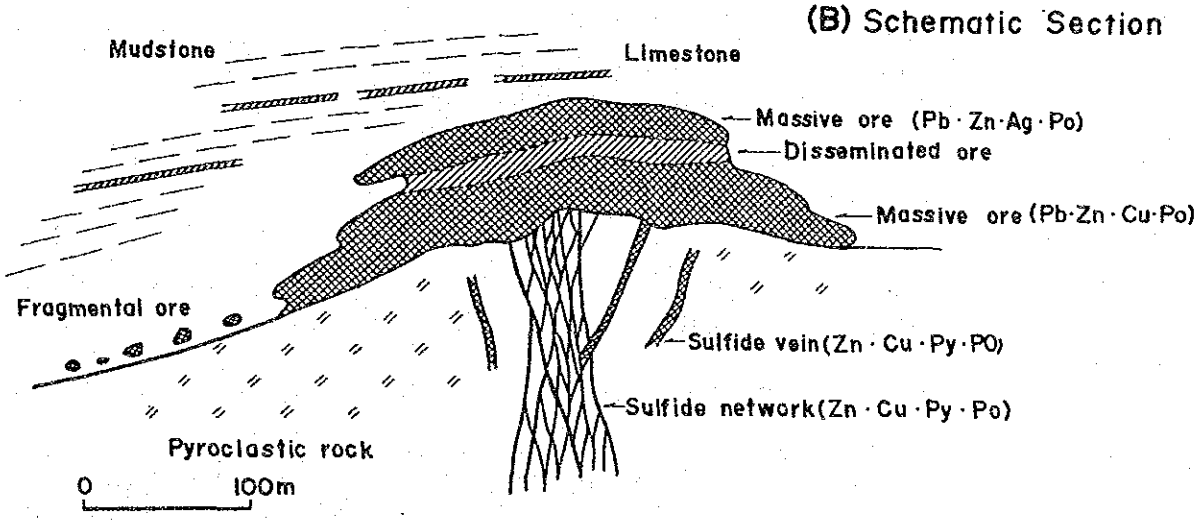

Fig 1-27 Genetic Model of the Hajar Ore Deposit

(A) Hajar Ore Deposit

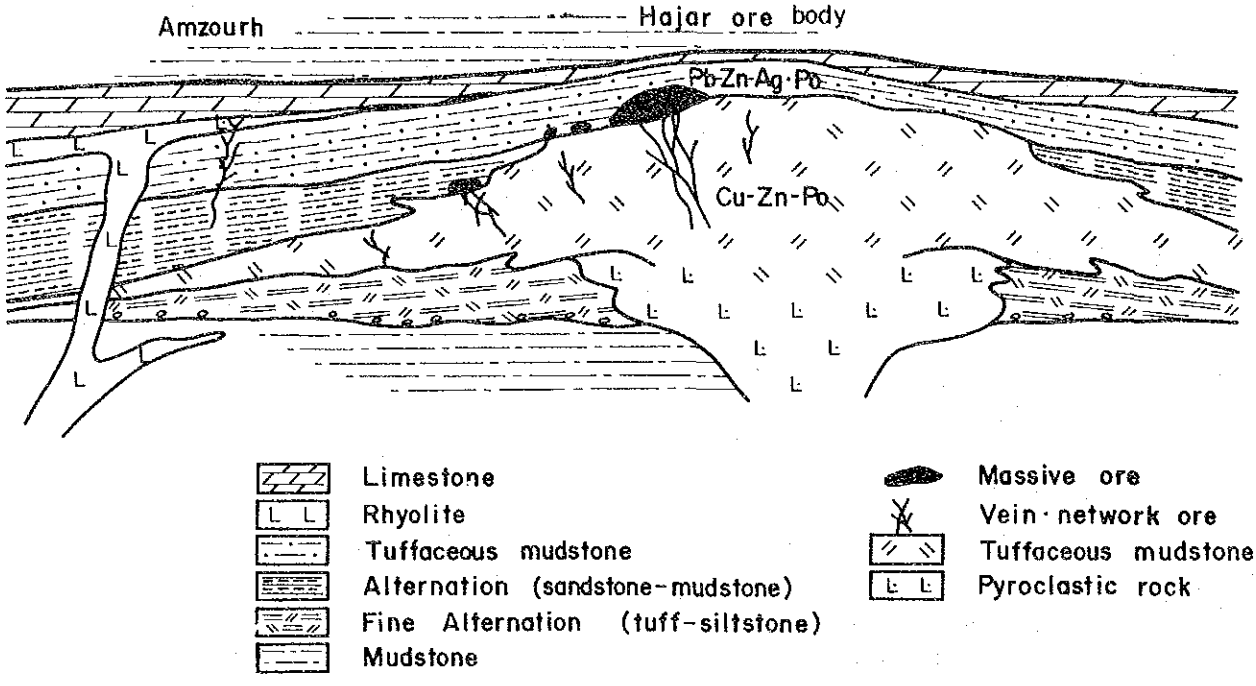

(B) Frizem Mineralized Zone

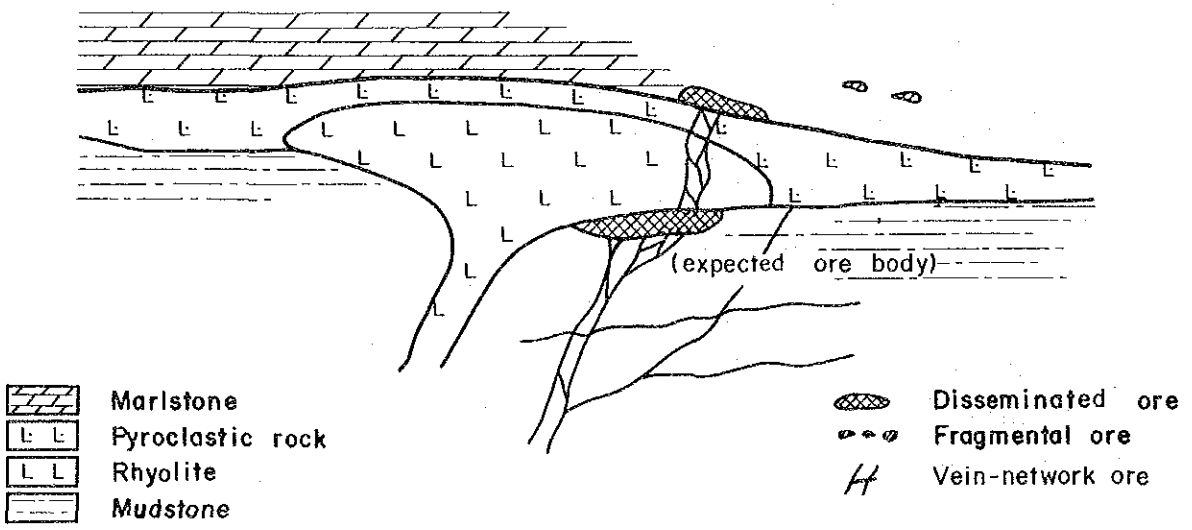

Fig. I-28 Schematic Cross Section of Ore Deposit

PARTICULARS

PART II

GEOPHYSICAL SURVEY

CHAPTER 1 OUTLINE OF THE SURVEY

Airborne magnetic survey was carried out in this survey area and the resulting magnetic anomaly was the key to the discovery of the Hajar ore deposit. But since then there were quite a few geophysical survey techniques carried out in the area which lead to the discovery of new ore deposit. During the Phase I survey, CSAMT measurements were carried out to find several low resistivity anomalies.

From the rock sample measurements (the resistivity and frequency IP effect of the Hajar ore minerals were about 20 ohm-m and 20 % respectively), the IP method was considered to be one of the effective geophysical tools. The density difference between Hajar ore (about 4.5 g/cm^3) and the background (about 2.7 g/cm^3) was so big that the gravity survey was also considered effective in this area. Therefore, IP and gravity surveys were carried out in the Phase II.

Principles, measurements and interpretation techniques of IP and gravity methods are explained in this chapter in addition to the actual measurement procedures and equipments used for the survey.

1-1 IP Method

1-1-1 Principles of IP Method

The induced polarization method is an electrical prospecting technique based on the phenomenon called induced polarization (IP), which is the electrochemical polarization occurs across the interface between electron-conducting mineral and ion-conducting pore solution.

Upon the application of the DC currents into the ground, voltage difference arises between two potential electrodes. When the currents turned off, that voltage difference sometimes would not suddenly goes to

zero but takes several seconds to minutes to decay to zero. On the contrary, when the currents are applied to the ground, it takes some time for the voltage difference to have constant value. This IP phenomenon is called time domain IP. And if IP effect is measured as a function of frequency, it is called frequency domain IP. Both time domain and frequency domain methods are equivalent theoretically, but have different features in practice. Since the frequency domain measurement was used for the project, the latter is explained mainly in this chapter.

The mechanism of IP phenomenon is not fully studied, but usually the explanation is done by the overvoltage and membrane polarization. The IP theory, measurement technique and interpretation methods are explained in detail by Sumner (1976) and Seigel (1967).

The frequency domain method is to measure the resistivities as a function of frequency. For example, the resistivities of sulfide minerals, graphite etc. are the functions of frequency as shown in the following figure.

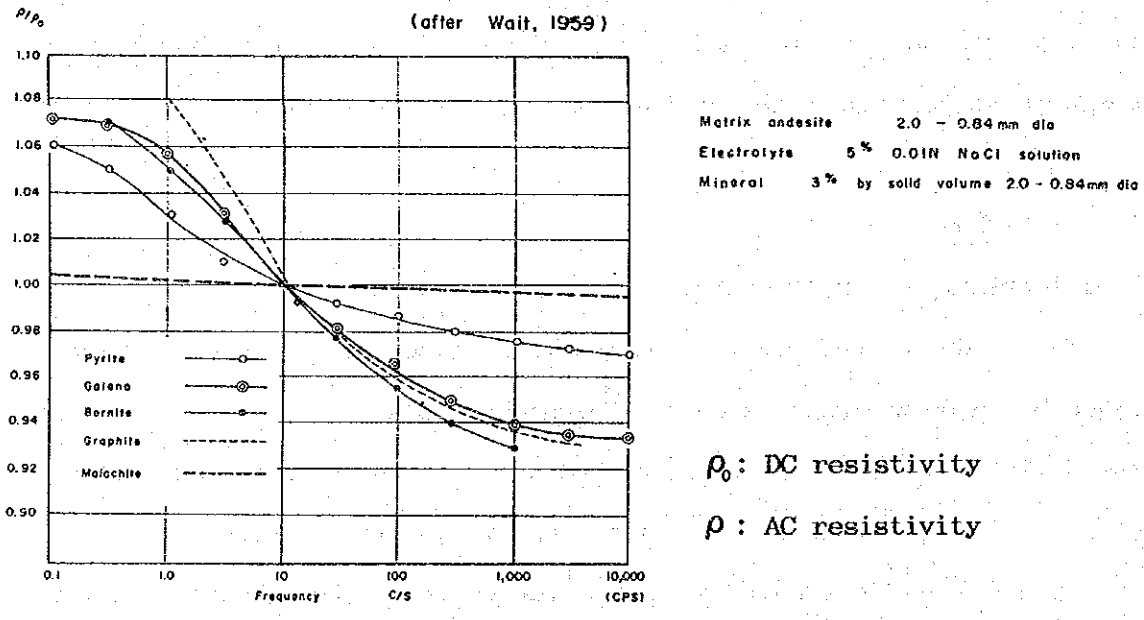

Resistivity of minerals as a function of frequency

The IP value (frequency effect FE) is defined by the two resistivity values measured by different frequencies as :

$$FE = \frac{R_1 - R_2}{R_2} \times 100\ (\%) \quad \cdots\cdots\cdots\cdots\cdots\cdots\cdots\cdots (1)$$

where R1 : apparent resistivity measured at lower frequency

R2 : apparent resistivity measured at higher frequency

There are some discrepancy among literatures related to the definition of FE, using R2 or $\sqrt{R1R2}$ as the denominator of equation (1), but no substantial difference exists.

The apparent resistivity values measured by a pair of potential electrodes are calculated by the following expression :

$$R = K \frac{\Delta V}{I} \quad (\Omega \cdot m) \quad \cdots\cdots\cdots\cdots\cdots\cdots\cdots\cdots (2)$$

where R : apparent resistivity (ohm-m)

K : geometric constant

I : applied current (A)

ΔV : measured voltage (V)

The dipole-dipole array as shown in the following figure is used very often for the IP measurement.

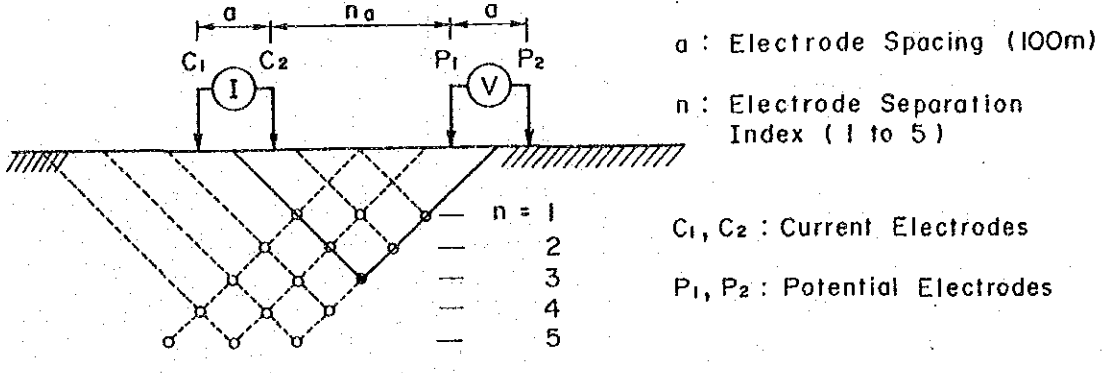

Dipole-Dipole Configuration

By using the dipole-dipole array of electrodes, coupling between the transmitter and the receiver can be reduced. The dipole length (a) of 100 m, and the separation (n) of 1 to 5 were used for the survey. The depth of the investigations increases as n increases, and approximately expressed as follows :

$$\text{the depth of investigation} = \frac{n+1}{2}\, a \qquad \cdots\cdots(3)$$

For example, the depth is about 100 m when n=1 and a=100 m, and about 300 m can be expected when n=5 and a=100 m.

It is possible to plot both apparent resistivity (as the function of n) and profiling data on a single two-dimensional diagram, giving a pseudosection of apparent resistivity along survey line. Resistivity values are plotted at the depth calculated from eq. (3) for the pseudo-section for this report.

And the electrode constant for the dipole-dipole array is calculated by the following equation :

$$K = \pi \cdot a \cdot n \cdot (n+1) \cdot (n+2) \qquad \cdots\cdots(4)$$

1-1-2 Resistivity and IP Measurement

(1) Measurement

Resistivity and IP values were measured in frequency domain using the dipole-dipole array of electrodes as stated earlier in this chapter. As the power source of the transmitter, a 50Hz engine generator was prepared for the survey. The generated 50Hz alternating currents were rectified and smoothed in the transmitter, and then transformed to very low frequency alternating currents by the SCR invertor circuits inside, which were applied to a pair of current electrodes.

A pair of non-polarizable potential electrodes were used to detect ground voltage differences, which were measured by a potentiometer inside the receiver after the filtration of unnecessary frequency noise components. Dry batteries were used for the power source of the receiver to minimize the noise.

IP and resistivity measurements consist of two parts, namely the land survey of measurement lines and actual measurements, and explained as follows :

1. Land Survey of the Measurement Lines

Laying out of the survey lines was carried out with an Ushikata pocket compass and measuring tapes. The intervals between measuring points were measured with the measuring tape, while azimuth and dipping angle were measured with the pocket compass. Each station sites was marked with a pile of stones, having corresponding painted station numbers on it.

2. Resistivity and IP Measurements

(a) Preparation of Current Electrodes and Wiring

As a current electrode, the steel plate of about 30 cm and 40 cm in dimensions was buried for each station at 50 cm to 1 m depth. By surrounding the electrode plate with the mixture of salt water (20 to 40 l) and Bentnite, the grounding resistance was reduced to 100 to 500 ohms.

Due to the very hard ground surface, one crew of 3 persons could make only average 3 electrode holes a day, the dimension of which is about 1 m wide, 1 m height and 50 cm to 1 m deep. 3 TO 4 crews of 3 persons were organized to make the holes in advance to the actual measurement process.

At the electrode site where the ground resistance was high, additional efforts were made like enlarging the holes and putting more salt water until the resistance was reduced to 100 to 500 ohms.

In order to minimize the measurement errors due to coupling between current and potential cables and leakage of currents, very careful wiring techniques like no intersection nor approach of cables, careful connections of cables to keep the insulating resistance maximum were performed at the field site.

(b) Potential Electrodes

Non-polarizable electrodes which had spiral copper wire submerged with copper sulfate solution was used as a potential electrode. Electrode polarization can be minimized by using the copper ions as the charges carrying currents at the copper electrode. Potential electrodes were also buried in the current electrode holes with 1 to 5 l of copper sulfate solution to reduce contact resistance between the electrode and ground to about 100 ohms to 1 kohm.

(2) Measuring Equipment

The specifications of measuring equipment used for the survey were as follows :

(a) Transmitter

Model L-5802, Manufactured by Yokohama Electric Lab.

Input power voltage	AC 90 V to 130 V
Output voltage	40 V to 800 V
Output currents	0.2 A to 4 A
Frequency	DC, 0.1, 0.3, 1.0, 2.5 Hz
output impedance	100 ohm to 4 kohm

(b) Receiver

Model DF-58Z, Manufactured by Yokohama Electric Lab.

Sensitivity	100 microvolts to 10 V 5 ranges
input impedance	2 Mohm
Resolution	sensitivity 0.1 to 1 %, FE 0.1 %
Noise	5 microvolts p-p input equiv.
Error	0.5 % FE 1 mV to 10 V

(c) Generator

Model EC2000X, Manufactured by Honda

Output power	2 kVA (60 Hz), 1.7 kVA (50 Hz)
Running time	2.5 hours continuous
Fuel capacity	3.3 l
Weight	37 kg (dry)

(3) Laboratory Measurement of Rock Samples

The rock samples were shaped to cube, and immersed in the water for about 24 hours before the measurements of rock properties. Samples were held between a pair of copper electrode plates. And the filter papers soaked in saturated copper sulfate solution were inserted between the sample and the electrode plate to minimize the contacting resistance. The current density within a rock sample was kept as close as possible to the actual current density, but minimum value was about 3 microampares/cm to maintain reasonable S/N ratio.

The measured rock properties are shown in Table II-2, and the location of sampling site is indicated in Fig.II-4. The average resistivity and FE values of Hajar ore samples were about 18 ohm-m and 15 % respectively. There were significant differences between those values and other rock samples like quaternary rocks (73 ohm-m, FE 1.1 %) and older rocks (510 ohm-m, FE 0.8 %).

The resistivity of pyrrhotite is as low as $2.0*10^{-6}$ to $1.6*10^{-4}$ ohm-m (Keller 1966). Due to the high resistivity matrix like quartz in which very conducting minerals are dispersing, total rock resistivity seems to be as high as 20 ohm-m.

1-1-3 Interpretation of Resistivity and IP data

(1) Pseudosection Plotting

Resistivity values were plotted at the midpoint of dipole-dipole array into five lines, to which the electrode separation n is corresponding. For example, the first line of apparent resistivity pseudosection is for n=1, and the second line is for n=2 and so on.

Topographic correction technique by computer 2D simulation is common to compensate the terrain effects in case of steep topography. This correction can not be applied in case of complicated or 3D topography, or not necessary for flat topography, which is the case of this survey area.

(2) Computer 2D Simulation

Computer 2D simulations were carried out for the survey lines which showed low resistivity and high IP anomalies. 2D finite element programs were used to interpret those survey lines.

At first, an initial model was introduced from the corresponding pseudosection, taking into account the results of past work including literatures, numerical calculations, water tank experiments and so on. Then numerical calculations were carried out for the model and construct the second model by comparing the results to the field data. The same process was continued until reasonable model, the numerical calculation of which created well represented the field data, was found. Sometimes, the results of these numerical simulation would not create the reasonable numerical model because of the 3D geological structure.

1-1-4 Specifications of the Measurements

Figure II-2 shows 13 survey lines (26.6 km) measured during the survey period. Length and the number of measurement points for each line are shown in the following table.

Block	Line Name	Length(km)	no.stations
Hajar	HJ-1	2.0	80
	HJ-2	2.0	80
Tiferouine	TF-1	2.0	80
	TF-2	1.5	55
	TF-3	2.0	80
Akhlij-Oukhribane	AK-1	3.6	160
	AK-2	1.5	55
Lamrah	LM-1	1.5	55
	LM-2	2.0	80
	LM-3	3.0	130
	LM-4	1.5	55
Frizem	FZ-1	2.0	80
	FZ-2	2.0	80
Total		26.6	1070

As for the electrode array, dipole-dipole array was used with the electrode separation a=100 m, and separation constants (n) were varied from 1 to 5. Maximum currents were tried to put into the ground, but average values of the currents were about 1 ampere.

2.5 Hz and 0.3 Hz were used for the measuring frequency, and apparent resistivities were calculated using the higher frequency.

1-2 Gravity Method

The procedure of the gravity survey is shown as the following flow-chart:

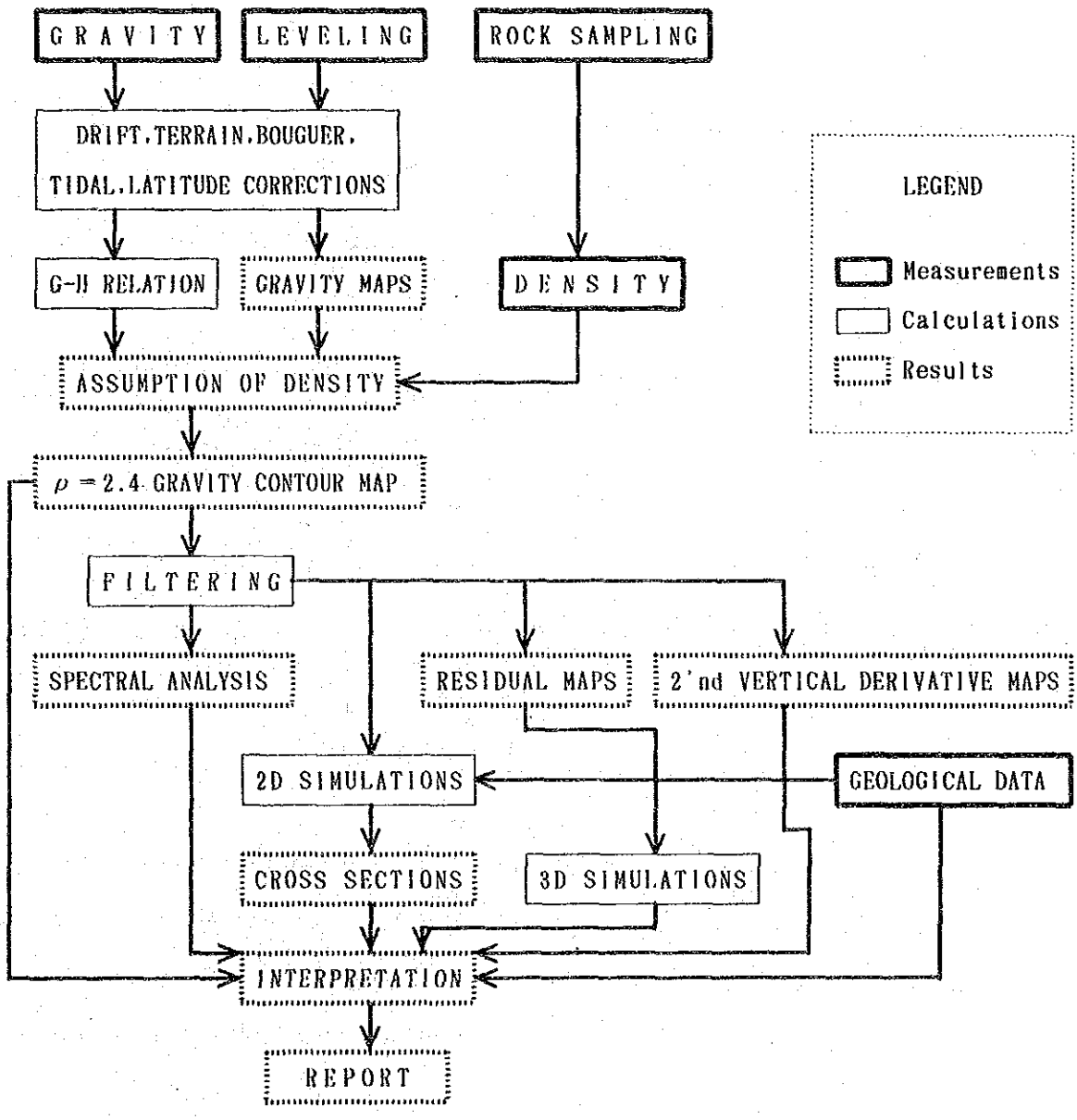

1-2-1 Gravity Stations

The location of the measured 745 gravity stations are shown in Fig.II-3. The stations located on the IP survey lines were measured at 100 m spacings. The stations surrounding the lines were distributed densely but further stations were sparsely distributed at the spacing of 200 to 400 m.

1-2-2 Gravity Measurements

(1) Gravimeter

Two gravimeters, G-283 and G-806 of Lacoste & Romberg, Inc. were used for the survey. The specifications are as follows:

TYPE	La Coste & Romberg,INC.Model G Geodetic Gravity Meter	
No.	283	806
Operation Range	0~7,386.54mgal	0~7,091.20mgal
Temperature	51.7 ℃	49.7 ℃
Reading Line	2.80	3.10
Date of Production	Jan.,1972	Feb.,1985
Dimensions	14×15×20 (cm)	17×15×22 (cm)
Meter Weight	8.6 kg	9.1 kg

These gravimeters have wide operating range of gravity values, from 0 mgal to over 7000 mgal. Due to the accuracy and stability of these gravimeters, monthly drift of which for example was less than 1 mgal, only one closure measurement per day was enough to obtain precise data.

(2) Standard Absolute Gravity Value

Utilized standard absolute gravity value was at the base station identified B73 established by B.R.P.M., located in front of Batiment de L'ONI on Avenue Poincare in Marrakech. The altitude and standard absolute gravity value had been defined as 456 m and 979,317.61 mgal respectively.

A temporally base station for closure measurement , named No.1000, was set in Residence Marrakech where the field survey office was settled. After two times of the closure measurements with the base station B73, the standard absolute value of the temporally base station was established to be 979,318.21 mgal (Tab.II-1). Since the base station B73 was defined using Potsdam system, measured gravity values in this survey were also closured with that system.

1-2-3 Leveling

The direct leveling method was adopted for all 745 stations by using Auto level B-2 of Sokkisha, Japan. Furthermore, the cross section levelling was also performed for one of the terrain corrections called sketch correction.

Two triangular points measured by Division de la Cartographie, Morocco, were used for the basements of leveling, the accuracy of which were as follows:

$$\varepsilon \leq 20 \sqrt{D}$$

where, ε: error of leveling (cm)

D: horizontal distance of leveling route (km).